

Titre: Computational Fluid Dynamic Modeling of a Hydraulic Flocculator
for the Charles-J.-Des Baillels Water Treatment Plant (City of
Title: Montreal)

Auteur: Nika Sarabi
Author:

Date: 2023

Type: Mémoire ou thèse / Dissertation or Thesis

Référence: Sarabi, N. (2023). Computational Fluid Dynamic Modeling of a Hydraulic
Flocculator for the Charles-J.-Des Baillels Water Treatment Plant (City of Montreal)
Citation: [Mémoire de maîtrise, Polytechnique Montréal]. PolyPublie.
<https://publications.polymtl.ca/57060/>

 **Document en libre accès dans PolyPublie**
Open Access document in PolyPublie

URL de PolyPublie: <https://publications.polymtl.ca/57060/>
PolyPublie URL:

**Directeurs de
recherche:** Benoit Barbeau, & Bruno Blais
Advisors:

Programme: Génie civil
Program:

POLYTECHNIQUE MONTRÉAL

affiliée à l'Université de Montréal

**Computational Fluid Dynamic Modeling of a Hydraulic Flocculator
for the Charles-J.-Des Bailleurs Water Treatment Plant
(City of Montreal)**

NIKA SARABI

Département des génies civil, géologique et des mines

Mémoire présenté en vue de l'obtention du diplôme de *Maîtrise ès sciences appliquées*

Génie Civil

December 2023

© Nika Sarabi, 2023

POLYTECHNIQUE MONTRÉAL

affiliée à l'Université de Montréal

Ce mémoire intitulé :

Computational Fluid Dynamic Modeling of a Hydraulic Flocculator for the Charles-J.-Des Baillets Water Treatment Plant (City of Montreal)

présenté par **Nika SARABI**

en vue de l'obtention du diplôme de *Maîtrise ès sciences appliquées*

a été dûment accepté par le jury d'examen constitué de :

Michèle PRÉVOST, présidente

Benoit BARBEAU, membre et directeur de recherche

Bruno BLAIS, membre et codirecteur de recherche

Mathieu LAPOINTE, membre

DEDICATION

*To the love of my life:
Javad.*

ACKNOWLEDGEMENTS

I would like to commence by expressing my heartfelt gratitude to my professor and research director, Benoit Barbeau. His exceptional teaching and supervision, vast expertise, and unwavering availability have played an instrumental role in my academic journey. Benoit, I'm profoundly thankful for entrusting me with the opportunity to work on such a pioneering project. Your dedication to your work and your ability to instill your passion for water treatment in others have been truly inspiring. Your encouragement and support throughout my master's degree have been invaluable. I appreciate your enthusiasm, kindness, and composure—they have made a significant difference.

Next, I extend my sincere appreciation to Bruno Blais for his substantial contributions to my project. Bruno, your support, availability, remarkable efficiency, and exceptional organizational skills have been indispensable. I have learned a great deal from you, and I'm genuinely grateful. Thank you for guiding me through the project.

Benoit and Bruno, I'm immensely thankful for the knowledge and expertise I have gained while working alongside both of you. It has been a privilege to have your combined wisdom supporting my project.

I would also like to express my gratitude to the entire staff of the Chair for creating a pleasant working environment and for their unwavering support and expertise. Julie, Jacinthe, Mirna, and Melanie, your contributions are deeply appreciated.

A special thank you goes to Yves and Tetiana for their invaluable assistance. Laura and Adèle, your help have made my life significantly easier on numerous occasions. I must extend my immense appreciation to Nariman for the support and guidance provided during this time.

I'm also grateful to my colleagues from the office and the friends I have made during my master's program who made this journey joyful for me: Ludovica, Marianne, Jerome, Aleks, Amélie, Hadia, and special thanks to my friend Eli for being there for me.

Lastly, I wish to thank my wonderful husband, Javad, and my family members for their unwavering support. Nima, Mom and Dad, thank you for your support.

RÉSUMÉ

Cette étude vise à fournir une solution durable et résiliente pour faire face aux impacts négatifs du changement climatique sur la qualité de la source d'eau de l'usine de traitement d'eau Charles-J.-Des Bailleys. Une fréquence accrue d'orages peut entraîner des augmentations significatives de la turbidité certains jours, entraînant une diminution de l'efficacité du processus de filtration. Par conséquent, l'utilisation d'un flocculateur hydraulique avant la filtration directe est proposée pour améliorer l'élimination de la turbidité et prolonger la durée des cycles de filtration. L'analyse du fonctionnement et de l'efficacité de ce flocculateur avec deux configurations (8 ou 16 chicanes) a été réalisée en utilisant la Dynamique des Fluides Numérique (CFD) à travers OpenFOAM, en plus d'une étude expérimentale pour définir la cinétique de croissance des floccs selon le nombre de Camp (Gt).

Les résultats indiquent que l'ajout de chicanes en amont des filtres peut créer efficacement la perte de charge nécessaire pour effectuer la floculation hydraulique. De plus, l'analyse de la vitesse a révélé des variations distinctes des schémas de flux et des longueurs de recirculation, la configuration à 16 chicanes montrant un flux plus cohérent et contrôlé, impactant potentiellement l'efficacité globale de la floculation.

En examinant le gradient de vitesse (valeur G), la configuration à 16 chicanes réduit significativement la plage de 10 s^{-1} à 500 s^{-1} , indiquant un meilleur contrôle du flux par rapport à la plage plus large, de 10 s^{-1} à plus de 1000 s^{-1} , observée dans le canal à 8 chicanes. De plus, une évaluation qualitative du nombre de Camp (Gt) illustre une augmentation notable de Gt après l'ajout de chicanes, le Gt actuel dans le canal sans chicane étant inférieur à 10,000, tandis que le canal à 16 chicanes connaît des valeurs de Gt plus élevées de 53,000, et la configuration à 8 chicanes a une valeur de Gt de 26,000 à la sortie du flocculateur, ce qui correspond à la plage inférieure de Gt généralement utilisée.

Les défis expérimentaux dans la mesure de la taille des floccs nécessitent de s'appuyer sur la microscopie, confirmant que l'augmentation du diamètre des floccs est associée à un Gt plus élevé. Par conséquent, la prédiction de la distribution de la taille des floccs en utilisant des données expérimentales et de simulation combinées indique une distribution de floccs dans

la plage de 30 à 60 μm pour les deux configurations, avec un pourcentage plus élevé de tailles de floccs plus importantes dans le canal à 16 chicanes.

En conclusion, bien que la configuration à 16 chicanes offre un meilleur contrôle du flux et des tailles de floccs anticipées plus grandes, les coûts de construction et la nécessité de tests à l'échelle pilote doivent être pris en compte pour une décision équilibrée entre des performances améliorées et un investissement accru. Il est recommandé de valider l'impact bénéfique de l'amélioration de la floculation sur la performance du filtre à l'échelle pilote.

ABSTRACT

This study aims to provide a sustainable and resilient solution to address the adverse impacts of climate change on the water source quality of the Charles-J.-Des Bailleurs water treatment plant. Increased occurrence of storms may lead to significant increases in turbidity on certain days leading to a decreased efficiency of the filtration process. Accordingly utilizing a hydraulic flocculator prior to direct filtration is proposed to improve turbidity removal and increase the length of filtration cycles. Analyzing the function and efficiency of this flocculator with two configurations (8 or 16 baffles) was performed utilizing Computational Fluid Dynamics (CFD) through OpenFOAM in addition to an experimental study to define flocs growth kinetics according to the Camp number (Gt).

The results indicate that adding baffles upstream from the filters can effectively create the necessary head loss to perform hydraulic flocculation. Moreover, velocity analysis revealed distinctive flow pattern variations and recirculation lengths, with the 16-baffle setup demonstrating a more consistent and controlled flow, potentially impacting overall flocculation efficiency.

Examining velocity gradient (G value), the 16-baffle configuration significantly narrows the range to from 10 s^{-1} to 500 s^{-1} , indicating superior flow control compared to the wider range, 10 s^{-1} to over 1000 s^{-1} , observed in the 8-baffle channel. In addition, qualitative assessment of Camp number (Gt) illustrates a notable Gt increase after adding baffles, the current Gt in the channel without baffle is lower than 10,000, while the 16-baffle channel is experiencing higher Gt values of 53,000 and the 8-baffle setup has the Gt value of 26,000 at the flocculator exit, which aligns with the lower range of typically used Gt.

Experimental challenges in floc size measurement prompt reliance on microscopy, confirming that increased floc diameter is associated with higher Gt. Consequently, predicting floc size distribution using combined experimental and simulation data indicates floc distribution in the range of 30 to 60 μm for both configurations, with a higher percentage of larger floc sizes in the 16-baffle channel.

In conclusion, while the 16-baffle configuration offers better flow control and larger anticipated floc sizes, construction costs and the need for pilot-scale testing should be considered for a

balanced decision between improved performance and increased investment. It's recommended that the beneficial impact of improved flocculation on filter performance be validated at the pilot scale.

TABLE OF CONTENTS

DEDICATION.....	III
ACKNOWLEDGEMENTS.....	IV
RÉSUMÉ.....	V
ABSTRACT.....	VII
TABLE OF CONTENTS	IX
LIST OF TABLES	XII
LIST OF FIGURES	XIII
LISTE OF SYMBOLS AND ABBREVIATIONS.....	XV
CHAPTER 1 INTRODUCTION.....	1
1.1 Context.....	1
1.2 Thesis organization.....	2
CHAPTER 2 LITERATURE REVIEW	3
2.1 Mechanism of Direct filtration.....	3
2.2 Flocculation.....	4
2.2.1 Factors affecting flocculation	5
2.2.2 Camp Number	11
2.2.3 Benefits of Flocculation in Direct Filtration.....	12
2.3 Computational Fluid Dynamics	12
2.3.1 Numerical Methods	13
2.3.2 Governing equations.....	13
2.3.3 Turbulence Models.....	14
2.3.4 CFD structure.....	16

2.3.5	SALOME software.....	16
2.3.6	OpenFOAM software	17
2.3.7	Application of CFD in flocculation.....	17
2.4	Conclusion	19
CHAPTER 3 OBJECTIVES AND HYPOTHESES		21
3.1	Objectives	21
3.2	Research Hypotheses.....	21
CHAPTER 4 MATERIALS AND METHODS.....		22
4.1	Overview of Charles-J.-Des Bailleys water treatment plant	22
4.2	CFD Model development and application.....	28
4.2.1	Configuration of numerical model.....	28
4.2.2	Development of Geometry	29
4.2.3	Mesh Generation	29
4.2.4	Configuration of OpenFOAM Numerical Model	31
4.3	Experimental studies	35
4.3.1	Overview of experimental protocol.....	35
4.3.2	Measurement of floc growth kinetics.....	37
CHAPTER 5 RESULTS AND DISCUSSION		44
5.1	CFD model application.....	44
5.1.1	Model Convergence	44
5.1.2	Velocity field analysis.....	48
5.1.3	Turbulent dissipation energy (ϵ)	49
5.1.4	Velocity Gradient (G value)	51
5.1.5	Camp number (Gt)	53

5.2	Floc kinetic experimental measurement	55
5.2.1	Laser diffraction Particle analyzer (Mastersizer 3000)	55
5.2.2	Direct Photometric Analyzer (Brightwell)	57
5.2.3	Microscopy	59
5.3	Results	60
CHAPTER 6 CONCLUSION AND RECOMMENDATIONS.....		64
6.1	Conclusion	64
6.2	Recommendations	65
REFERENCES..		67

LIST OF TABLES

Table 2-1. Raw water eligibility criteria for Direct Filtration (AWWA, 1980).....	4
Table 4-1. Contact time calculations for channels between mixing zone and filters.....	25
Table 4-2. Baffles design parameters	27
Table 4-3. descriptions of meshes for mesh independence assessment	31
Table 4-4. Calculated parameters for turbulence model.....	33
Table 4-5. Water characteristics.....	36
Table 4-6. Jar-test protocol	37
Table 5-1. Convergence test results	46
Table 5-2. Head loss comparison from simulation and target head loss	51
Table 5-3. Mastersizer 3000 test protocol	56
Table 5-4. Bright well test protocol.....	58
Table 5-5. Microscope test protocol.....	59
Table 5-6. The predicted floc size at the end of the flocculator.....	62

LIST OF FIGURES

Figure 2-1. Mechanisms of coagulation and flocculation (Kurniawan et al., 2020).....	5
Figure 2-2. Factors affecting Coagulation and Flocculation processes.....	6
Figure 2-3. Types of Flocculator: (a) Hydraulic (b) Mechanical.....	7
Figure 2-4. CFD structure needed to reach the numerical modeling solution.....	16
Figure 4-1. Schematic of the Water Treatment Process at DesBaillets water treatment plant (City of Montreal).....	22
Figure 4-2. Coagulant injection point at the effluent channel of raw water pumps (see Fi. 4-3) .	23
Figure 4-3. Schematic of filtration stage	24
Figure 4-4. Layout of filtration stage	25
Figure 4-5. Flocculation channel with 8 baffles (plan view).....	28
Figure 4-6. Flocculator geometry: (a) Without baffle (b) With baffles	29
Figure 4-7. Generated mesh for channel (a) without baffle (b) with 8 baffles	30
Figure 4-8. The CFD analysis process (Shaw, 1992).....	34
Figure 4-9. Compute Canada Chart for Running a Simulation on Cedar Cluster	35
Figure 4-10. Jar-test.....	37
Figure 4-11. Mastersizer 3000	38
Figure 4-12. Brightwell Technologies INC's DPA 4100.....	39
Figure 4-13. Protocol of sample measuring with Brightwell technology (DPA 4100).....	41
Figure 4-14. Olympus BX51 microscope.....	42
Figure 4-15. Captured images using microscopy.....	43
Figure 5-1. Specified lines in the flocculator geometry for mesh convergence analysis	45

Figure 5-2. Mesh quality influence over the magnitude of velocity over (a) line 1 and (b) line 2..	44
Figure 5-3. Residuals of CFD simulation for the channel with 8 baffles.....	47
Figure 5-4. Residuals of CFD simulation for the channel with 16 baffles.....	47
Figure 5-5. Velocity profiles (in $\text{m}\cdot\text{s}^{-1}$) in the flocculator with (a) 8 baffles and (b) 16 baffles ...	48
Figure 5-6. Epsilon variation (in $\text{m}^2\cdot\text{s}^{-3}$) in the flocculator (a) without baffle (b) with 8 baffles (c) with 16 baffles	50
Figure 5-7. Epsilon distribution in the channel with 8 and 16 baffles	50
Figure 5-8. G value in the flocculator (a) without baffle (b) with 8 baffles (c) with 16 baffles...	52
Figure 5-9. Cumulative frequency distribution of G value in the channel without and with baffle	53
Figure 5-10. Gt value in the flocculator (a) without baffle (b) with 8 baffles (c) with 16 baffles	54
Figure 5-11. Gt values at the exit of the flocculator in the channel without and with baffle	55
Figure 5-12. Results of floc diameter measurement employing Mastersizer 3000.....	56
Figure 5-13. Mastersizer 3000	57
Figure 5-14. Results of floc diameter measurement employing Brightwell ($G=50 \text{ s}^{-1}$).....	58
Figure 5-15. Results of floc diameter measurement employing Brightwell ($G=100 \text{ s}^{-1}$).....	58
Figure 5-16. Results of floc diameter measurement employing microscopy	60
Figure 5-17. Floc diameter (μm) distribution in the flocculator (a) with 8 baffles (b) with 16 baffles.....	61
Figure 5-18. Cumulative frequency distribution of flocs diameter in the flocculator with baffle	61

LISTE OF SYMBOLS AND ABBREVIATIONS

AWWA	American Water Works Association
CFD	Computational Fluid Dynamics
DOC	Dissolved Organic Carbon
FDM	Finite Difference Method
FEM	Finite Element Method
FVM	Finite Volume Method
GCI	Grid Convergence Index
HPC	High-Performance Computing
LES	Large Eddy Simulation
MELCC	Ministère de l'Environnement et de la Lutte contre les changements climatiques
NOM	Natural Organic Matter
PDEs	Partial Differential Equations
RANS	Reynolds-Averaged Navier-Stokes
SIMPLE	Semi-Implicit Method for Pressure Linked Equations
TOC	Total Organic Carbon
UV	Ultraviolet
WHO	World Health Organization
WTP	Water Treatment Plant

CHAPTER 1 Introduction

1.1 Context

Fresh water is one of the most important and valuable substances on Earth, it's truly remarkable to consider that less than three percent of Earth's water is fresh and accessible. What's even more astounding is that most of this small percentage is not easily within reach. A significant portion, approximately 68 percent, exists in the form of ice caps and glaciers, while another 30 percent lies beneath the Earth's surface as groundwater. The remaining fraction, a mere 0.3 percent, is what we find in lakes, rivers, and swamps. (National.Geographic, 2023). A report from UNICEF and the World Health Organization (WHO) reveals that more than half of the world's population doesn't have access to clean drinking water, proper sanitation, and good hygiene (WHO, 2019).

Drinking water treatment plants are developed and studied in the field of civil engineering, they are essential structures to achieve the quality requirements established by the reference regulations. The treatment may require physical, chemical, and biological operations and processes for the transport and handling of the fluid, making it necessary to build different structures within the treatment plant for its application. The Commencement of the Charles-J.-Des Baillels factory dates to 1973 and it offers a daily production capacity of 1,136,000 m³ /d, supplying approximately 60% of Montreal Island's average water consumption. (Bouchard, 2017) The treatment process at the Des-Baillels plant is designed with a sequence of direct filtration, ozonation, UV treatment, and chlorination. The plant traditionally relies on direct filtration without coagulation due to consistently good raw water quality. However, during periods of intense winds in the fall or spring snowmelt, there is a notable decline in water quality and consequently an increase in turbidity levels. Given that filtration is the only mechanism for turbidity removal, this presents a significant challenge for the plant. To tackle this issue, a coagulation process was introduced before the filtration stage. Despite this modification, the observed results have not met the anticipated improvements in filter performance, especially during peak periods. The filter cycles have decreased to 16 hours, and the capacity for filter washing is limited to two filters at a time, even though there are 60 filters in operation.

This work mainly concerns the improvement of existing infrastructures by the addition of a hydraulic flocculator prior to direct filtration employing Computational Fluid Dynamics (CFD), to meet the requirements for ensuring the sustainability and resilience of the plant in the face of emerging concerns, such as the impact of climate change on water source quality.

The flocculator is an important hydraulic structure, whose function is to give enough energy to the fluid. This energy promotes the collision of colloidal particles that have been destabilized during the coagulation stage, leading to the formation of larger flocs. These enhanced flocs can then be efficiently removed through decantation or filtration processes. Therefore, the flocculator, like any hydraulic structure, must be analyzed and handled technically, considering important parameters such as retention time and velocity gradients, pressure drop, and baffles specifications.

These parameters are traditionally obtained through tests carried out in a laboratory and through fluid flow government equations. However, the results obtained through these equations only give a global idea of the flocculator. Therefore, numerical simulations have been implemented recently, providing a relatively straightforward way to analyze different scenarios compared to physical experimentation. These simulations utilize Computational Fluid Dynamics (CFD) programs, OpenFOAM software, which work through iterative solutions of the Navier-Stokes equations governing fluid flow.

1.2 Thesis organization

This thesis is divided into six chapters. Chapter 1 serves as an introduction, laying out the reasons for conducting this study. Chapter 2 focuses on a literature review, explaining the fundamental concepts of flocculation, direct filtration, and application of Computational Fluid Dynamics (CFD) in designing hydraulic flocculators. Chapter 3 outlines the research objectives and hypotheses. Moreover, an overview of the experimental methods used in the project, along with the techniques applied in CFD simulations is provided in Chapter 4. Furthermore, Chapter 5 presents and analyzes the results, covering both experimental and numerical findings. Finally, chapter 6 concludes the thesis with a summary of the findings and offers recommendations for future research.

CHAPTER 2 Literature Review

This literature review centers on the application of flocculation processes to enhance the performance of downstream filtration. Specifically, this literature review focuses on flocculation in direct filtration, starting with a brief explanation of direct filtration and flocculation process. Furthermore, it explores the impact of flocculation in direct filtration and examines the kinetics of flocculation. Additionally, the second part of the review focuses on the application of Computational Fluid Dynamics (CFD) in studying flocculator design, along with examination of previous studies with a similar objective.

2.1 Mechanism of Direct Filtration

Direct Filtration is presented as a viable alternative for conventional surface water treatment process. One of the defining characteristics of direct filtration is the absence of sedimentation process before the filtration. Like any other procedure, there are advantages and drawbacks for this method. Direct filtration system offers cost reduction in terms of operation and maintenance and capital expenditures due to elimination of settling tanks. In addition, the chemical dosage and flocculation time are lower to form filterable small flocs known as “Pin flocs” rather than forming larger settleable flocs. On the other hand, one of the notable disadvantages is to offer less operational flexibility and dependence on one single process for removal of all types of particulate matter. In the absence of sedimentation, the filtration must be capable of responding to variation of water quality and that is why there is a reasonable limitation on the types of water that can be treated using direct filtration (Culp, 1977; L. D. V. Melo, Barroso, Figueiredo, Costa, & Oliveira, 2021). Proper application of direct filtration is significantly dependent on raw water specifications such as turbidity, color, density of algae and concentrations of coliforms (Dalsasso & Sens, 2006). In the Design Guide for Drinking Water Production Facilities of Quebec (MELCC 2019) the raw water eligibility criteria for direct filtration has been published based on (AWWA, 1980) guidelines:

Table 2-1. Raw water eligibility criteria for Direct Filtration (AWWA, 1980)

Parameter	Turbidity (NTU)	Color (unit)	Algae (units/ml)	Iron (mg/L)	Manganese (mg/L)
Value	<5	<40	<2000	<0.3	<0.05

Conventional filtration has good operational flexibility and is suitable for most surface waters; however, it entails more sludge production and construction costs. On the other hand, direct filtration is a more compact and efficient process but it is limited to high-quality waters showing no variation in terms of turbidity. In direct filtration, the process begins with coagulation-flocculation and then directly goes to the filtration step, in certain situations the flocculation tank is omitted as well, which process commonly known as in-line or contact filtration (Post, Atherholt, & Cohn, 2011). In the current configuration, the Charles-J.-DesBaillets water treatment plant (Montreal) which will be the topic of this research can be assimilated to an in-line direct filtration process.

2.2 Flocculation

Raw water found in nature contains different impurities such as colloidal particles and dissolved natural organic matter (NOM). Flocculation plays a crucial role in the treatment of drinking water. Following the coagulation process, which destabilizes particles primarily characterized by negative or positive charges, the introduction of flocculation chemicals facilitates the aggregation of smaller, destabilized particles into larger clusters known as flocs. The coagulant dose is largely dependent on the NOM concentration, where a higher concentration requires the use of a higher coagulant dose which is detrimental to filter operation.

Flocs are subsequently removed through filtration or sedimentation, with the goal of reducing turbidity and color in the water (Crittenden, Trussell, Hand, Howe, & Tchobanoglous, 2012). Flocculation can be further understood through the mechanisms of orthokinetic and perikinetic flocculation. Orthokinetic flocculation occurs when particles collide and aggregate due to fluid motion or shear forces. This mechanism relies on the relative movement of particles caused by

flow conditions. Perikinetic flocculation, on the other hand, involves the agglomeration of particles through Brownian motion or diffusion. In this mechanism, random particle motion leads to proximity and adhesion (McEwen, 1998). As shown in Figure 2-1 during floc formation, various processes, such as charge neutralization, sweep coagulation, bridging, and patch flocculation, can take place. (Kurniawan et al., 2020)

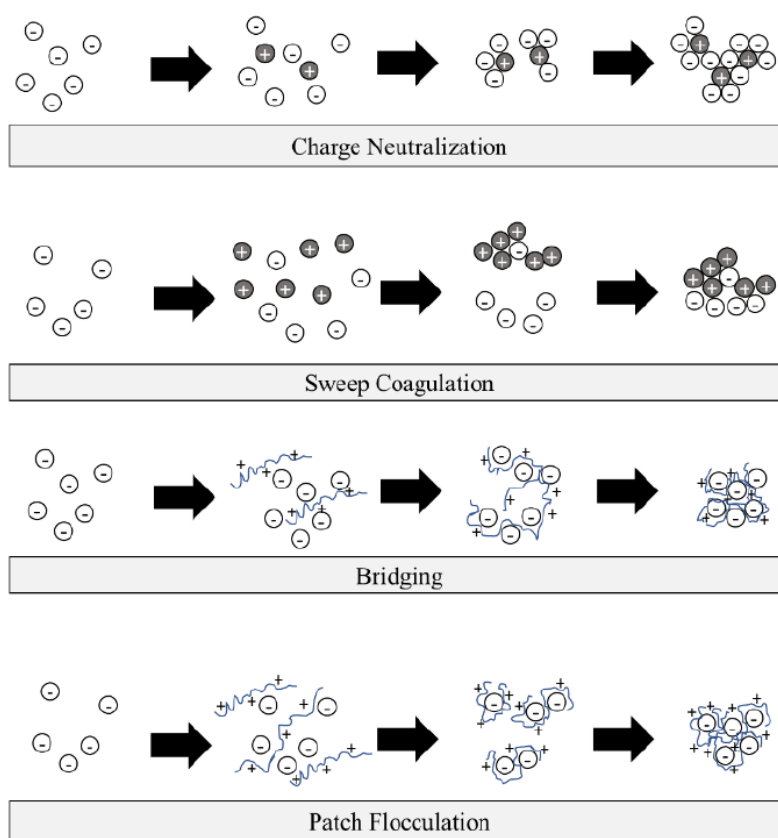


Figure 2-1. Mechanisms of coagulation and flocculation (Kurniawan et al., 2020)

2.2.1 Factors Affecting Flocculation

Numerous studies have examined the impact of various parameters on the flocculation process. Figure 2-2 illustrates a diagram depicting some of these relevant investigations, followed by a brief description of the factors which impact flocculation.

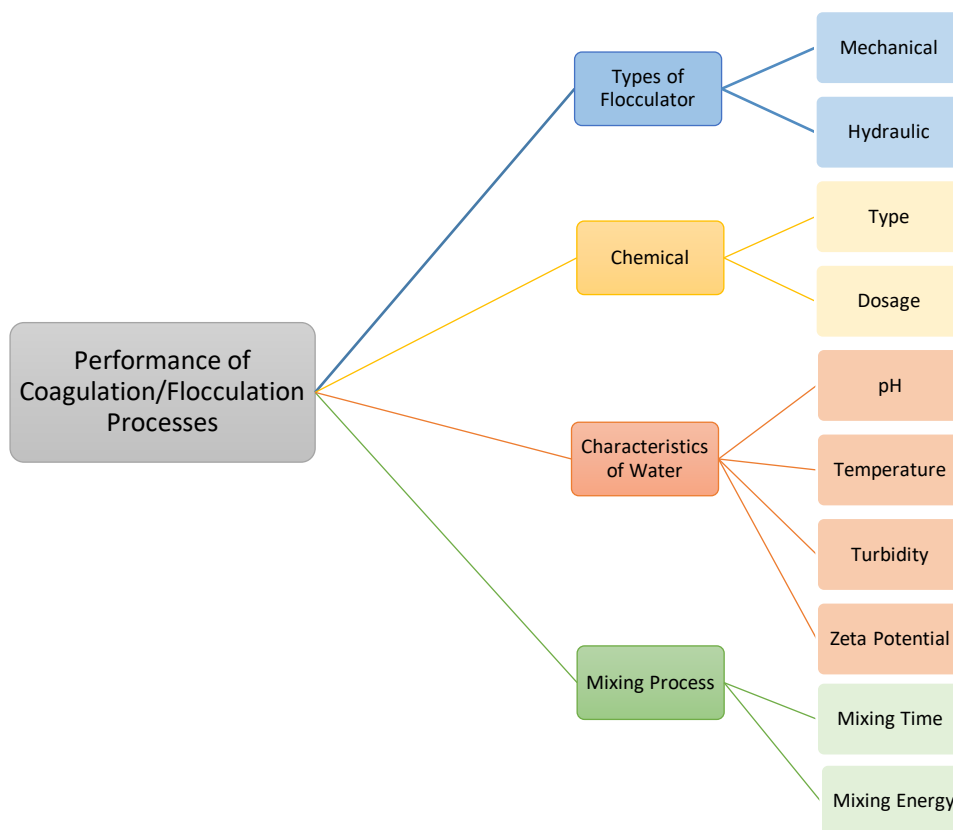


Figure 2-2. Factors affecting Coagulation and Flocculation processes

2.2.1.1 Type of Flocculator

In water treatment plants, the flocculation process can be achieved using mechanical or hydraulic methods. The main difference lies in the type of energy input. The mechanical flocculators get the required shear stress via an agitator by supplying energy input. On the other hand, hydraulic flocculators rely on the energy provided from head loss across the baffles. (Jonathan Bridgeman, Jefferson, & Parsons, 2009) The two types of flocculator are demonstrated schematically in Figure 2-3. (Egarr, Horton, Rice, & Hunter, 2016) The hydraulic flocculator can be either horizontal or vertical, it is widely held that hydraulic flocculators with around-the-end baffled channels are inflexible and complex to design (J. Haarhoff, 1998). However, the research of J. Haarhoff (1998) regarding horizontal flocculators and evolving of design equations, showed that a remarkable level of flexibility is attainable in both design and operational aspects of flocculators with around the end baffles. (J. Haarhoff, 1998) In Des-Baillets case study

considering the conditions of the existing channel, the selected flocculator is the horizontal hydraulic flocculator.

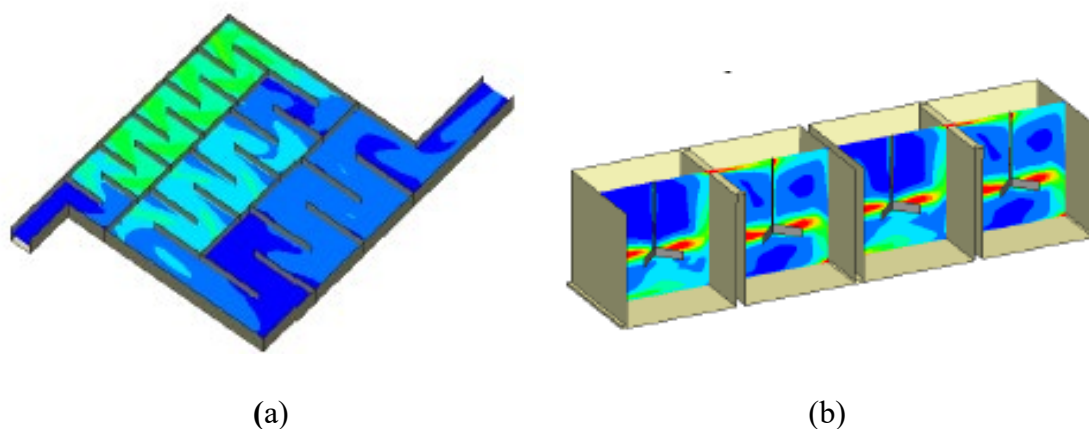


Figure 2-3. Types of Flocculator: (a) Hydraulic (b) Mechanical

The primary factors influencing hydraulic flocculator design are the intensity of agitation and contact time. In the case of a hydraulic flocculator with baffles, the G-value (intensity of agitation) is determined using Eq 2-1. Here, ΔH represents the head loss across the channel, and 't' accounts for the contact time. Typically, hydraulic flocculators operate with contact times ranging from 10 to 30 minutes and head losses between 0.3 and 0.9 meters (Kawamura, 2000).

$$G(s^{-1}) = \sqrt{\frac{\rho \times g \times \Delta H}{\mu \times t}} \quad \text{Eq 2-1}$$

2.2.1.2 Chemicals (coagulants/flocculants)

The processes of coagulation and flocculation require the addition of compounds known as coagulants and flocculants, these chemicals can be classified into two main types: organic and inorganic. The nature of chemicals is such that inorganic coagulants are metal-based such as aluminum or iron salt, while organic coagulants are polymer-based, mostly epi-DMA or polyDADMAC. Floc size can be increased by using an appropriate polyelectrolyte; a dense floc with a regular shape is preferable (Kurniawan et al., 2020). Flocculants, such as polyacrylamide, are not usually used in direct filtration applications given that the objective is not to produce

settleable flocs. Traditionally, alum was widely used in the coagulation process. A study was conducted to assess the performance of alum compared to various polyaluminum chloride coagulants (PACls) to treat raw water with low turbidity and pH of approximately 8. These studies demonstrated that PACls are equally or more effective than alum in direct filtration and do not require pH adjustment during coagulation and flocculation (Zarchi, Friedler, & Rebhun, 2013). Furthermore, another study illustrated that for water supplies with low turbidity and low to moderate Total Organic Carbon (TOC) levels, using direct filtration with cationic polymers is a viable treatment method. This approach is particularly effective for waters with TOC concentrations of 5 mg/L or lower. (Edzwald, Becker, & Tambini, 1987) Meanwhile, the optimal dosage of chemicals should be assessed case by case.

2.2.1.3 Water Characteristics

This has been known for decades that, coagulation and flocculation process is heavily influenced by the pH of the sample given that coagulants are most effective in certain pH ranges. Furthermore, Jar test experiments of (Fitzpatrick, Fradin, & Gregory, 2004) were conducted to investigate the effect of temperature on flocculation using different coagulants. The results showed that temperature impacts the size, strength, and reforming ability of flocs. Higher temperatures lead to larger flocs that have reduced breaking and reforming abilities at lower temperatures. In addition, coagulation and flocculation are affected by the concentration of suspended particles and NOM initially present in water. These chemicals tend to work best in high-turbidity water, and they are less effective in low-turbidity conditions. It may be necessary to use a coagulant or flocculant aid in cases of extreme turbidity, which would render direct filtration inapplicable. Additionally, the characteristics of suspended particles and NOM, including their zeta potential, play a crucial role in coagulation and flocculation performance. (Kurniawan et al., 2020)

2.2.1.4 Mixing Time and Intensity

Mixing plays a key role in coagulation/flocculation process, it starts with flash mixing to disperse the products properly and initiate coagulant hydrolysis, followed by a slow mix in order

to increase the probability of collision between smaller flocs and create larger aggregates. Bouyer, Line, Cockx, and Do-Quang (2001) present three main findings in their studies regarding to mixing velocity and residence time in the water treatment process. Firstly, it demonstrates that a higher velocity gradient leads to a reduction in terminal floc size due to breakage. Secondly, it reveals that higher mixing speeds, significantly shorten the time required to reach steady state. Lastly, the study observes that the floc size initially tends to increase and then decreases, due to the influence of flocs erosion due to shear stress. In addition, the duration that a floc particle is exposed to a specific velocity gradient during the flocculation process is crucial. Different zones within the process may subject a particle to varying G (velocity gradient) values, and the time spent in each zone can significantly impact the outcome of the flocculation process. (Ducoste, Clark, & Weetman, 1997) to minimize flow short-circuiting in the process.

The kinetics of flocculation are crucial in understanding the aggregation behavior of colloids. Flocculation involves bringing coagulated colloids into contact with each other, leading to the formation of larger aggregates. The mechanism of particle destabilization and subsequent colloid aggregation is complex and is acknowledged as a two-stage process involving particle transport and particle attachment. During the initial stage, agglomerating particles must undergo collisions, while in the second stage, they must adhere upon collision (Amirtharajah & O'melia, 1990; Jarvis, Jefferson, Gregory, & Parsons, 2005). In the flocculation process flocs do not keep growing, but they reach a steady size under a certain shear rate. It is generally believed that floc growth is limited by floc breakage, so the rate of floc formation and breakage is seen as a balance (Ducoste & Clark, 1998). In the classical expression, the rate of flocs growth (R_{floc}) depends on how often particles collide and how they interact. This can be described using Eq 2-2 as the difference between the rate of aggregation and the rate of floc breakage (R_{br}). The rate of aggregation can be calculated by multiplying the rate of particle collision (R_{col}) by a collision efficiency factor (α). The factor ' α ' represents the proportion of collisions that lead to attachment.

$$R_{floc} = \alpha R_{col} - R_{br} \quad \text{Eq 2-2}$$

The efficiency of collisions is variable and relies on the effective shear rate and particle size (Brakalov, 1987). (Von Smoluchowski, 1917) Initially introduced a comprehensive explanation

of particle collision using few simplifying assumptions. However, the analysis was limited to following assumptions:

- 1- no breakage of flocs is taking place.
- 2- all particles are same size and spherical before and after collision.
- 3- each collision only occurs between pairs of particles.
- 4- collision efficiency factor (α) is equal to one for all collisions.

The collision frequency between particles in orthokinetic flocculation with diameters of d_i and d_j in a two-dimensional flow can be derived using the following equation:

$$\beta(d_i, d_j) = \frac{\partial U}{\partial Y} \frac{(d_i + d_j)^3}{6} \quad \text{Eq 2-3}$$

Furthermore, Smoluchowski provided solutions to the set of differential equations for both perikinetic and orthokinetic flocculation. The solution for orthokinetic flocculation was determined as follow:

$$N_t = N_0 \exp \left(\frac{4}{\pi} \left(\frac{du}{dy} \right) \varphi t \right) \quad \text{Eq 2-4}$$

Where, N_t and N_0 are number of particles at time t and 0 respectively, $\frac{du}{dy}$ is fluid shear velocity and φ being volume fraction of particles, is assumed to be constant and calculated as $(4/3)\pi r^3 N_0$ (Thomas, Judd, & Fawcett, 1999). Consequently, (Camp, 1943) has developed the Smoluchowski equation by introducing their own expression of fluid's root-mean-square velocity gradient (G) and substitute it with the fluid shear velocity, $\frac{du}{dy}$:

$$\beta(d_i, d_j) = G \frac{(d_i + d_j)^3}{6} \quad \text{Eq 2-5}$$

And consequently, the Smoluchowski equation can be presented as Eq 2-6.

$$N_t = N_0 \exp (4/\pi) G \varphi t \quad \text{Eq 2-6}$$

In this approach, as it is depicted in equation 4, the G is a function of kinematic viscosity (ν), power input in the system (P) and the volume (V):

$$G = \sqrt{\frac{P}{\rho V \nu}} \quad \text{Eq 2-7}$$

P is regulated by dissipation of overall kinetic energy in the system. In the laminar flow, the dissipation energy happens due to the viscosity and friction between fluid layers, whereas in turbulent flow the modified expression for G is shown in equation Eq 2- 8.

$$G = \sqrt{\frac{\varepsilon}{\mu}} \quad \text{Eq 2- 8}$$

the dissipation energy mainly occurs due to the turbulent motion. Accordingly, they have established dissipation rate of turbulent kinetic energy (ε) as the power per unit mass ($p/\rho V$).

2.2.2 Camp Number

Camp and Stein's work in 1943, which investigated velocity gradients, led to the development of the Camp number (Gt). This number continues to be extensively used for designing flocculators in water treatment applications. For optimal flocculation, it is advisable to maintain a Camp number ranging from 3×10^4 to 2×10^5 (Kawamura, 2000). A higher value, resulting from excessive mixing or too long contact time would be a risk of floc shearing. During a pilot investigation of (Vigneswaran, Notthakun, & Thanh, 1984) involving direct filtration in natural water with kaolin, the ideal flocculation duration ranged between 3 to 10 minutes, corresponding to mixing intensities from 30 to 50 s^{-1} . Moreover, Bernhardt and Schell (1993) Han and Lawler (1992) work, suggested that using a G value just high enough to keep particles in suspension in flocculation units would let Brownian motion work effectively. If the energy input is too low, causing low particle concentration and particles not staying in suspension, there won't be enough particle collisions. In addition, Ball, Carriere, and Barbeau (2011) research highlights the fact that Gt can be consider as a predictor of flocculation in terms of flocs diameter.

2.2.3 Benefits of Flocculation in Direct Filtration

The advantages of incorporating flocculation must effectively being assessed case-by-case studies. However, it is a common practice to introduce a brief flocculation period of approximately 10 minutes before filtration (Post et al., 2011). The primary expected advantages of flocculation include enhanced water quality and extended cycle times. The experiments illustrate that direct filtration with coagulation and sufficient flocculation time can result in reliable turbidity removal equal to those achieved by conventional treatment, the optimal combination of flocculator and filter can result in uniform floc sizes and consistent head loss distributions throughout the filter's depth (Treweek, 1979). For efficient filtration, it is adequate to have flocs in the range of 10-50 μm given that larger flocs tend to quickly clog the filter, especially by creating a surface mat, resulting in a significant increase in head loss (McEwen, 1998). Moreover, as indicated by (Vigneswaran et al., 1984), under similar coagulation and mixing conditions, the turbidity of filtered water decreases as the flocculation duration increases. Dalsasso and Sens (2006) research depict that pre-flocculation showed benefits in increasing filtration cycle durations by 23 percent. However, the success of its implementation relies on the choice of coagulant and the filter medium's attributes. Additionally, pre-flocculation led in improvement of filtered water quality, particularly concerning color and turbidity. Additionally, Edzwald et al. (1987) experiment confirmed that, using direct filtration with flocculation resulted in a noticeable reduction in head loss compared to in-line direct filtration.

2.3 Computational Fluid Dynamics

In recent years, technology and computer science progress have led to the growth of a new aspect of fluid mechanics. This is called computational fluid dynamics (CFD). Computational Fluid Dynamics (CFD) solve the equation of fluid dynamics to predict the flow patterns within processes. These equations, known as the Navier-Stokes equations along with related turbulence transport equations, are solved together. This method is widely used to simulate complex three-dimensional flows around intricate shapes across various engineering fields related to fluid dynamics. (Andoh, 2006) Mentioned that the significant advantage of utilizing CFD in all industries is less reliance on costly models leading to propose of optimized model at an economical price. Moreover (Yeung, 2001) believes that CFD has overt advantage on the

physical model due to elimination of subjective interpretation of outcome. Nonetheless, CFD is very useful to understand fluid behavior, but it has its own limitations, according to (Van der Walt, 2002) “The CFD model will always remain as an approximation of reality.”

2.3.1 Numerical Methods

Multiple physical phenomena are described by Partial Differential Equations (PDEs). These equations are particularly challenging to solve due to their reliance on several independent variables, their nonlinear nature, and the requirement for accurate boundary and initial conditions. Consequently, only a handful of PDEs have solutions that can be found analytically. Therefore, numerical methods are like a guide for scientists and engineers to illuminate the path into the study of these PDE-defined physical processes. These methods involve approximating solutions at specific points within a function’s domain. This approximation is achieved through discretization, wherein unknown derivatives in each PDE are replaced with algebraic estimates. (Moin, 2010) Several variations of this fundamental approach exist such as Finite Difference Method (FDM), Finite Volume Method (FVM) and Finite Element Method (FEM). However, the finite volume method is particularly prevalent in computational fluid dynamics (CFD) simulations and engineering due to its suitability for describing equations under a conservation principle.

The FVM was initially conceived as a distinct version of finite difference formulation. By employing the integral representation of conservation equations and effectively managing intricate geometries, this approach becomes a wise choice in diverse scientific and engineering applications, where precision and adaptability hold significance. In the finite volume method (FVM), a fluid area is divided into cells forming a mesh. Each cell approximates solutions for equations in the computational grid using data from neighboring cells. Boundary and initial conditions are applied for cells at the domain edges and initial time step, ensuring accurate results. (Moukalled et al., 2016)

2.3.2 Governing Equations

According to the context of classical mechanics, it’s wise to commence the study with fundamental laws such as conservation of mass, momentum, and energy. When a conservation of

mass or momentum is applied to a volume of control with constant density, it leads to the derivation of the incompressible continuity and Navier-Stokes equations respectively in their differential form as follows:

$$\nabla \cdot \vec{U} = 0 \quad \text{Eq 2-9}$$

$$\rho \left(\frac{\partial \vec{U}}{\partial t} + \vec{U} \nabla \cdot \vec{U} \right) = -\nabla p + \mu \nabla^2 \vec{U} + \rho \vec{f} \quad \text{Eq 2-10}$$

In this context, $\vec{U} = \vec{U}(x, t)$ represents the velocity vector of the fluid, varying with time and space, ρ represents fluid density and μ stand for viscosity, $f = f(x, t)$ signifies body force and $p = p(x, t)$ is pressure.

Using the finite volume method and an adequate discretization, the Navier-Stokes equations can be solved in time and space to obtain the pressure and velocity fields.

2.3.3 Turbulence Models

Computational fluid dynamics (CFD) use turbulence models to simulate and predict turbulent flow behavior. Fluids in turbulent motion undergo rapid fluctuations in velocity, pressure, and other properties. Turbulence models fall into three main categories:

- 1- RANS (Reynolds-Averaged Navier-Stokes) Models.
- 2- LES (Large Eddy Simulation) Models
- 3- Hybrid Models (combination of RANS and LES)

RANS models statistically average turbulent behavior, balancing accuracy and efficiency for a wide range of applications. LES models resolve larger turbulent structures, providing more detailed insights but demanding higher computational resources. The focus of this study involves the utilization and examination of the RANS models.

The Boussinesq hypothesis is the basis for several turbulence models to represent turbulent viscosity, μ_t , based on velocity () and length scale (ℓ) as shown in equation Eq 2-11 (Moukalled et al., 2016)

$$\mu_t = \rho \ell \sqrt{k} \quad \text{Eq 2-11}$$

With

$$k = \frac{1}{2} \overline{\mathbf{v}' \cdot \mathbf{v}'} \quad \text{Eq 2-12}$$

The effects of turbulence can be captured using these models without explicitly resolving all turbulent structures in the flow, which would be computationally costly and impractical. In these models, additional equations describe how turbulence quantities evolve over time and space, allowing them to provide a method for describing the statistics of turbulence. The models can be categorized in four base groups (Zero- Equation Model, One- Equation Model, Two Equation Models and Second Order Clouser Models), the advantages and strengths of each group of models differ, which is why no one model can be applied universally across all flow situations.

Among them, Two-Equation Models are widely preferred in engineering applications, in this approach, the turbulent velocity and length scales are determined by solving two distinct transport equations. One equation is dedicated to turbulent kinetic energy (k), while the other addresses the turbulence length scale or an equivalent parameter (such as ε , which indicates the dissipation of turbulence kinetic energy per unit time, or ω , representing the rate at which turbulent energy dissipates). These equations include the creation, dispersion, and termination of turbulence within the flow pattern. The main presumption for these models is that the flow remains close to local equilibrium and that the Reynolds number is sufficiently high to ensure local isotropy. (Jonathan Bridgeman et al., 2009) The common turbulence models included with commercially accessible CFD packages are typically standard k - ε model, the renormalized group k - ε model (RNG k - ε), the standard k - ω model, and the shear-stress transport (SST) k - ω model and Reynolds Stress Model (RSM). In the present study the standard k - ε model was employed due to analyze the changes in local velocity distribution, turbulent kinetic energy (k), and turbulent kinetic energy dissipation rate (epsilon). The K-epsilon turbulent model has been chosen for a variety of computational fluid dynamics (CFD) simulations in the context of water treatment flow assessment. The K-epsilon model alongside its simplicity and reasonable computational cost, is capable of adequately capture the turbulence intensity and mixing

characteristics that are essential for understanding the flocculation process. The model is well established and practical choice for simulating in systems like flocculators, it is especially suitable for simulating internal flows. (Jonathan Bridgeman et al., 2009; Joodi, 2013)

2.3.4 CFD structure

The CFD structure consists of three parts in order to reach a solution; Figure 2-4 shows the structure that is carried out in all Computational Fluid Dynamics (CFD), starting with a pre-process that is input data, followed by the processing that is the part of the software to culminate with the post-process where you get the results to be analyzed and visualized.

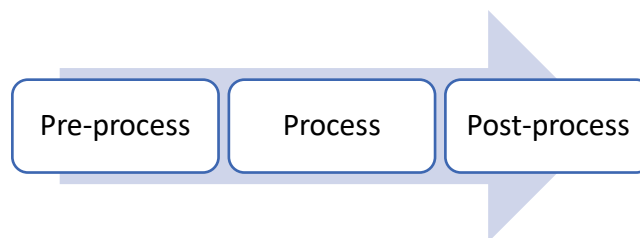


Figure 2-4. CFD structure needed to reach the numerical modeling solution

2.3.5 SALOME Software

Salome is an open-source software platform for numerical simulations in engineering and science that provides extensive pre- and post-processing tools. SALOME is highly user-friendly and widely used in order to creation and manipulation of complex 3D geometries and mesh generation, Salome facilitates the post-processing setup and visualization of simulations as well. The use of Salome is often accompanied by other simulation tools and solvers, such as OpenFOAM, Code_Aster, and Elmer, in order to provide a complete simulation workflow from geometry creation through post-processing. In this study, the Salome software is employed to carry out geometry modeling and mesh generation for the baffles. (SALOME-platform, 2019; SALOME, 2021)

2.3.6 OpenFOAM software

The OpenFOAM (Open-Source Field Operation and Manipulation) software package simulates and solves complex fluid flow and heat transfer problems numerically. It is free and open source. (OpenFOAM, 2022) The OpenFOAM software package includes solvers, libraries, and tools for performing CFD simulations in a wide variety of fields, including aerodynamics, heat transfer, chemical engineering, water treatment and more. Some of the key features of OpenFOAM include solver flexibility, open-source nature, meshing, parallel computing, post-processing and vibrant user community, where users share their experience, tutorials and problem-solving approaches in order to collaboration and learning. (OpenFOAM-Guide, 2020)

The OpenFOAM solution is fully complemented by ParaView's OpenFOAM reader module, which allows visualization of OpenFOAM solutions with elements that are commonly used in CFD, ParaView (ParaView, 2023) makes it easy for users to create animations by using these elements.

2.3.7 Application of CFD in flocculation

Designing flocculation processes has traditionally been based on empirical research and laboratory experiments. However, Computational Fluid Dynamics (CFD) has emerged as a significant achievement in science. Researchers and engineers can now simulate fluid flow, turbulence intensity, and mixing dynamics in flocculation systems using CFD. The application of CFD revolutionizes the understanding, prediction, and enhancement of flocculation. Several researchers have shown that computational fluid dynamics (CFD) can be used to predict orthokinetic flocculation in mechanical and hydraulic systems, demonstrating that it is a reliable method for describing local energy dissipation within a system. (Bilde, Hærvig, & Sørensen, 2023) In this section, a selection of prior studies that have utilized CFD for designing flocculation processes is highlighted.

(Joodi, 2013) conducted a simulation to examine how baffle geometry influences turbulence and particle interactions in hydraulic flocculators utilizing COMSOL software and $k-\varepsilon$ model. It reveals that longer baffles increase turbulence structures, thicker baffles decrease turbulence kinetic energy, and semicircular baffles promote more turbulence. The model finds that the

number of baffles and water inlet location in addition to inlet water velocity significantly impacting the results.

In the thesis of (S. Carlston, 2015) For the purpose of determining the best baffle configuration, 30 CFD simulations were performed, involving varying channel widths, baffle lengths, and flow orientations. Based on the results, baffle lengths should be aligned with the channel width of the tank, ensuring approximately equal openings. In this research the FLUENT software was employed and as turbulence model the (RNG) $k-\varepsilon$ was selected.

Ridgeman et al. (2008) employed CFD to study the local velocity gradient. In order to simulate the shear caused by a mechanical stirrer in a flocculation tank, the authors developed a Reynolds-averaged Navier Stokes (RANS) model for a single-phase steady-state local velocity gradient. subsequently an aggregate's strength and breakage were expressed in terms of the local velocity gradient based on experimental and numerical data obtained.

(Saha, Biswas, Nath, & Singh, 2021) used Computational Fluid Dynamics (CFD) to analyze the flow, within a channel by changing the number and shape of baffles using FLUENT and $k-\varepsilon$ turbulence model. The main findings indicate that the recirculation area changes based on baffles distance, height and thickness. Interestingly whether the baffles are flat or trapezoidal does not seem to affect how the flow behaves upstream. It's worth noting that in cases where flat baffles are used there are points where the flow speeds can reach, up to 3.22 times of inlet velocity.

(Johannes Haarhoff & van der Walt, 2001) Applied CFD to optimize the design of the hydraulic flocculator. The first step was verifying real flow velocities against theoretical CFD results, which established a reliable correlation and enabled continued CFD use in the study. The main aspect of the study is focused on the instability of the energy dissipation rate in the channel, which results in the variability of the G value. The study shows that the edge of the baffles is the critical zone with a high dissipation rate and G value, which leads in a high floc breaking in the specified area.

(John Bridgeman, Jefferson, & Parsons, 2010) study illustrated how CFD can be successfully used in water treatment flocculation process. According to the research findings the hydraulic flocculator revealed the presence of recirculation loops and stagnant areas, within the flocculation cells located between baffles. In addition, The G value exhibited significant variation through the

channel. The velocity gradient value was found to be higher, towards the edges of the baffles and on the walls opposite, to them.

According to (de Oliveira & Donadel, 2019), the assessment of G involves creating prototypes, which can be a costly process, and empirical equations can also be used as a quick way to assess G , but they can often be incompatible with the geometry of the unit, leading to a high number of errors. The research has a proven track record for calculating G values using CFD in water and wastewater treatment processes, including flocculation. In this study CFD results for helical coil hydraulic flocculators were compared with empirical equations for determining G values in six distinct cases that showed a promising correlation.

In (Ghawi, 2018) work on hydraulic flocculators with varying ratio of channels width to baffles spacing, the turbulent kinetic energy dissipation rate was calculated using ANSYS Fluent to find the optimal design of flocculator in terms of uniformity of energy dissipation rate. The outcome results assisted in determining factors such as baffle spacing, number of baffles, velocity gradient, residence time, and flocculation efficiency. Furthermore, to validate the results, a hydraulic flocculator was designed based on CFD results and predictably, the results were similar, and the design parameters were relatively accurate. Which confirms the application of CFD for designing hydraulic flocculators.

2.4 Conclusion

Direct filtration stands out as a viable alternative to the conventional surface water treatment process. It is widely accepted to introduce a brief flocculation prior to direct filtration in order to improve turbidity removal and extend the filters cycle. Additionally, experiments confirm the significant reduction of head loss in direct filtration with flocculation compared to in-line filtration. The velocity gradient, G value, is a crucial parameter in flocculation as it determines the intensity of mixing and influences the collision and aggregation of particle. Moreover, residence time (t) dictate how long particles remain in the flocculation zone. Therefore, the right balance of camp number (Gt) is essential for effective flocculation.

While conventional design of flocculation processes has been rooted in empirical research and laboratory experiments, the advent of Computational Fluid Dynamics (CFD) has revolutionized modeling and design practices. Studies have shown that CFD offers a dependable means of

predicting orthokinetic flocculation in both mechanical and hydraulic systems, offering a precise tool for characterizing local energy dissipation. Incorporating CFD into the design process not only enhances the accuracy and efficiency of flocculation systems but also facilitates precise calculation of crucial parameters such as velocity gradient and residence time, allowing for the design of various channels and baffles to evaluate results and select the optimal condition.

CHAPTER 3 Objectives and Hypotheses

3.1 Objectives

The main objective of the study is to assess how to design a hydraulic flocculator at the Charles-J.-Des Bailleys Water treatment plant (city of Montreal) to improve the turbidity removal and increase the duration of the cycles of filtration.

The specific objectives are:

1. Optimize the coagulation/flocculation process to increase the size of the floc at the Charles-J Des Bailleys plant.
2. Define the kinetics of floc formation in the laboratory according to flocculation condition (Gt).
3. Identify where would be the best location to install a hydraulic flocculator within the existing infrastructures,
4. Design a flocculator for the Charles-J Des Bailleys factory employing CFD and use the model to forecast the Gt at the channel effluent.

3.2 Research Hypotheses

The specific hypotheses to meet the objectives mentioned above are as follow:

1. The Mastersizer can measure the floc size.
2. Higher Gt values in the flocculation process will lead to an increase in floc diameter, indicating a positive correlation between energy input and floc size.
3. The presence of baffles will change the flow pattern and result in higher Gt value in the channel.
4. An increase in the number of baffles in the channel will lead to higher Gt value.

CHAPTER 4 Materials and Methods

This chapter covers the project's methodologies in three parts. First, it offers an overview of Charles-J.DesBaillets water treatment plant. Then, it outlines the computational fluid dynamic methods used to design the hydraulic flocculator for the Charles-J.DesBaillets water treatment plant and the last section explains the experimental methods used for performing laboratory-scale tests at CREDEAU to measure the flocs growth kinetics.

4.1 Overview of Charles-J.-Des Baillets Water Treatment Plant

The Des Baillets water treatment plant, designed in 1979, is depicted in Figure 4-1 follows a sequential process: starting with a low-pressure pump, proceeds to in-line filtration, followed by ozonation and UV treatment, and concludes with chlorination before the water is pumped in the distribution system. This WTP is the second largest operated by the City of Montreal and one of the largest in Canada. The plant traditionally employed direct filtration without coagulation due to generally good raw water quality. UV disinfection was added in 2008 to increase parasite removal while coagulation was initiated in 2010-2020 period in order to increase turbidity removal. Coagulation injection was initially scheduled to be conducted seasonally (during high turbidity events) but has since been conducted on a routine basis.

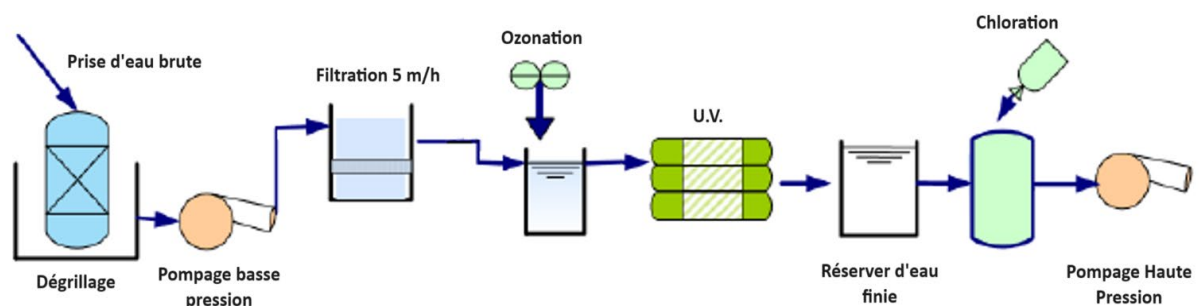


Figure 4-1. Schematic of the Water Treatment Process at DesBaillets water treatment plant (City of Montreal)

The water intake of the Des Bailleurs plant is in the St. Lawrence River, 500 meters from the shore, at the exit of Lake St. Louis. Due to this positioning, the raw water quality is partially influenced by the Ottawa River during some periods of the year. This influence is increased during periods of flooding, particularly in the spring. Storms and strong winds observed in the fall can also lead to sediment resuspension in Lake St. Louis. Since the filtration is the only mechanism for turbidity removal, when variations in the raw water composition are observed such as turbidity peaks, the filtration cycle declines. Backwashing capacity of filters is limited to 2 filters at a time while 60 filters are in operation. To address the events of turbidity, an upgrade was implemented in 2010 by introducing a coagulation process prior to filtration. However, this decision necessarily reduced the filtration cycle length given the improved solids capture in the filters.

As it is depicted in Figure 4-2, the coagulant is introduced directly into the water and there is minimal head loss in the channel to promote flocculation. Almost 90 percent of the total head loss between the flash mixing area and the filters takes place at the control valve along the way. This particular valve, with a velocity gradient of 1500 s^{-1} , leads to a head loss of approximately 1.07 meters (Bouchard, 2017). This project aims to design a hydraulic flocculator prior to the filtration process to enhance turbidity removal and extend the filter cycle as flocculation has been shown (cf chap. 2) to favor the growth of flocs which, in turn, reduces the head loss inside granular media filters.



Figure 4-2. Coagulant injection point at the effluent channel of raw water pumps (see Fi. 4-3)

The first step involves identifying an appropriate location for the flocculator. In Figure 4-4, the layout of the filtration stage is depicted. The pump is located at the left corner and after the addition of coagulant the water splits in two separate streams and, furthermore, each of them is divided to two channels, resulting in 4 identical area of 15 filters for a total of 60 filters.

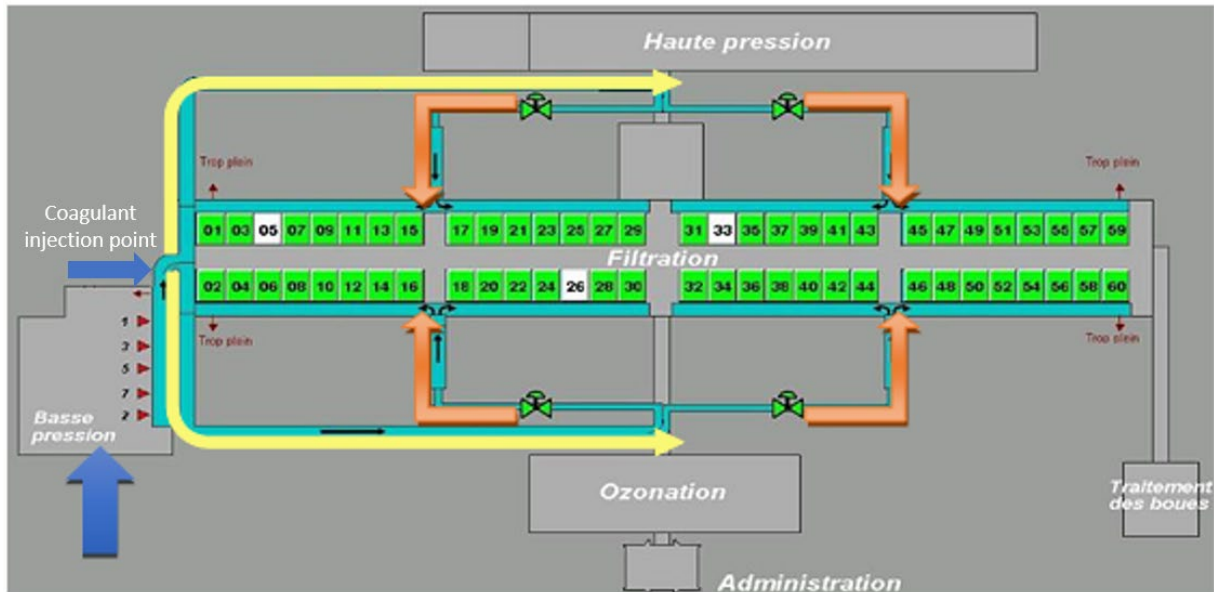


Figure 4-3. Schematic of filtration stage

The flocculator must be situated between the mixing area and the entrance of the filters in one of the available channels. The Figure 4-4 is illustrated the layout of filtration stage, the target channel is divided into four sections to provide a clearer understanding of the situation. As shown in the Table 4-1 the present contact time for each section was calculated individually. There are two options for the placement of the flocculator: before or after the control valve (in purple on Fig 4-4). In the flow rate of $3.16 \text{ m}^3 \cdot \text{s}^{-1}$, the longer channel before the valve (combining section 1 and section 2) provides a total contact time of approximately 8 minutes, while the shorter channel after the valve (combining section 3 and section 4) offers a contact time of about 5 minutes.



Figure 4-4. Layout of filtration stage

Table 4-1. Contact time calculations for channels between mixing zone and filters

	Length	Cross section Area	Volume	Flow rate	Detention time	Detention time
Unit	(m)	(m ²)	(m ³)	(m ³ s ⁻¹)	(s)	(min)
Section 1	77.895	11.88	925	6.32	146	2.44
Section 2	182.14	11.88	2163	6.32	342	5.70
Section 3	34.82	5.95	207	3.16	66	1.09
Section 4	50.60	12.26	620.5	3.16	196	3.27
Valve chamber	41.8	4.67 - 2.63	116	3.16	36	0.61

Selecting the longer channel before the valve poses a higher risk of floc breakage while passing through the valve. Additionally, constructing the flocculation on-site would require shutting down half of the filters. On the contrary, choosing the four shorter channels located after the control valves, with 5 minutes of contact time, ensures that the formed flocs are less likely to be disrupted by the valve and on-site construction would only require shutting down one quarter of

the filters. Taking all factors into consideration, the decision was made to utilize the shorter channel with 5 minutes of contact time as the channel for the design of a hydraulic flocculator.

The subsequent phase involves the design of baffles for the flocculator. According to the (Kawamura, 2000), the target head loss is set at 75 cm, so the head loss for each baffle was calculated for a different number of baffles as outlined in the Table 4-2. This was followed by determining the flow velocity while passing through the baffle using the minor head loss equation shown in Eq 4-1. Due to the substantial distance between the baffles, the flow pattern would be helicoidal rather than a 180-degree turn, as a result, K which stands for head loss coefficient was considered to be equal to 1.5 according to J. Haarhoff (1998). Moreover, the width of the baffle considered 0.1 m, as mentioned in Saha et al. (2021) study, high baffle thickness results in more water recirculation length in the flocculator. Furthermore, the slot width is computed and allows us to derive the appropriate size for the baffles. For this study and according to the achieved information, two scenarios were investigated: 8 and 16 baffles. A higher number of baffles allow for a more progressive energy dissipation but increases the construction costs.

$$\Delta h = K \frac{V^2}{2g} \quad \text{Eq 4-1}$$

Which V = average velocity in channel (m/s), Δh = head loss across each baffle (m), K = head loss coefficient, and g stands for gravitational acceleration (m/s^2).

The plan view layout of the selected channel with the installed baffles is illustrated in Figure 4-5 All dimensions are presented in meters and the layout was created using AutoCAD.

Table 4-2. Baffles design parameters

Number of baffles	Head loss in each baffle	Velocity in each baffle	Slot width (available space for water to pass)
n	H (m)	V (m.s ⁻¹)	B (m)
6	0.125	1.279	1.013
8	0.094	1.107	1.170
10	0.075	0.990	1.308
12	0.063	0.904	1.432
14	0.054	0.837	1.547
16	0.047	0.78	1.66

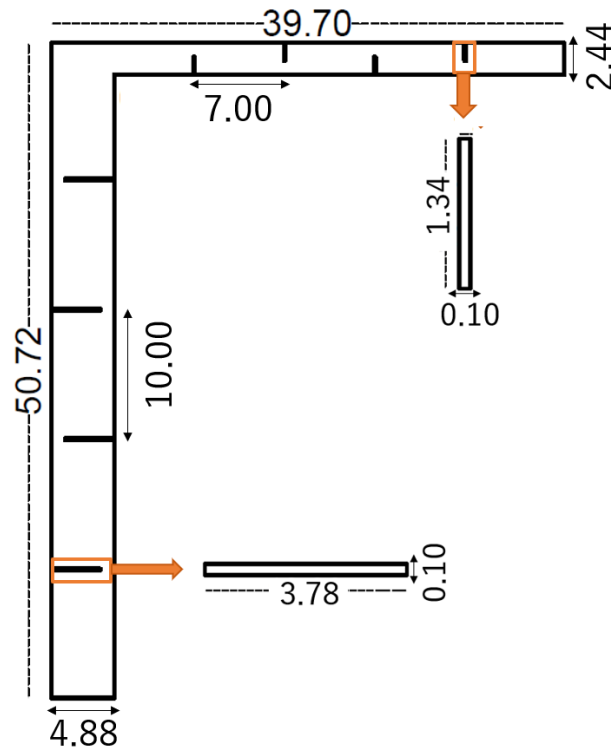


Figure 4-5. Flocculation channel with 8 baffles (plan view)

4.2 CFD Model development and application

4.2.1 Configuration of numerical model

Computational Fluid Dynamics (CFD) were employed to simulate the flow pattern in the hydraulic flocculator. The design of the flocculator with baffles and mesh creation was accomplished using SALOME and OpenFOAM software. (OpenFOAM, 2022; SALOME, 2021) Following the simulation, Paraview software was used to visualize and analyze the results (ParaView, 2023).

4.2.2 Development of Geometry

The computational domain was designed to replicate the actual channel dimensions of the Des Baillets water treatment plant, accounting for variations in baffle number and size. The primary channel structure was generated using the *blockMesh* feature in OpenFOAM, while the baffles were modeled using SALOME software. The geometry created with SALOME was exported with the format (. stl) to use for the next step. An illustration of the flocculator's geometry, both without baffles and configured with eight baffles, is provided in a 3D plan view in the Figure 4-6.

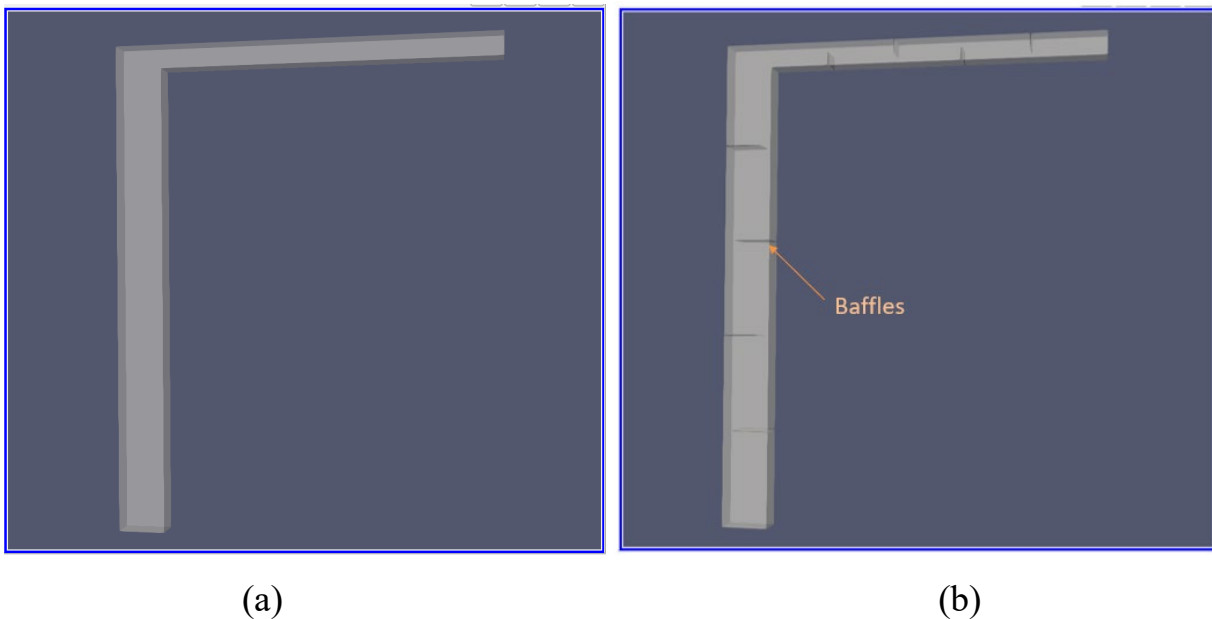


Figure 4-6. Flocculator geometry: (a) Without baffle (b) With baffles

4.2.3 Mesh Generation

While working with Computational Fluid Dynamics (CFD), it is crucial to consider a precisely defined geometry, accompanied by a high-quality mesh. The quality of the mesh plays a vital role since the results of the simulation are directly influenced by it. The mesh generation process for this study involved a dual-step approach utilizing *blockMesh* and *snappyHexMesh* techniques.

As a basic representation of the computational domain, blockMesh was initially used to create the primary structured mesh. Additionally, basic topology and boundary patches of the domain were defined during this phase, each face of the blocks was assigned a specific name, a critical step that would later enable the application of comprehensive boundary conditions. In this project, the inlet and outlet of the model is defined as *patch* type and additionally lower walls, upper walls, front and back walls are assigned as type *wall*.

Following that, *SnappyHexMesh* was introduced to refine the mesh, capturing finer details and addition of baffles to the channel. This tool enabled the creation of a high-quality mesh with refined boundary layers, improving flow representation accuracy. A combination of blockMesh and snappyHexMesh will result in a more accurate simulation (reference). Here you can see the channel mesh with eight baffles and without baffles in the Figure 4-7.

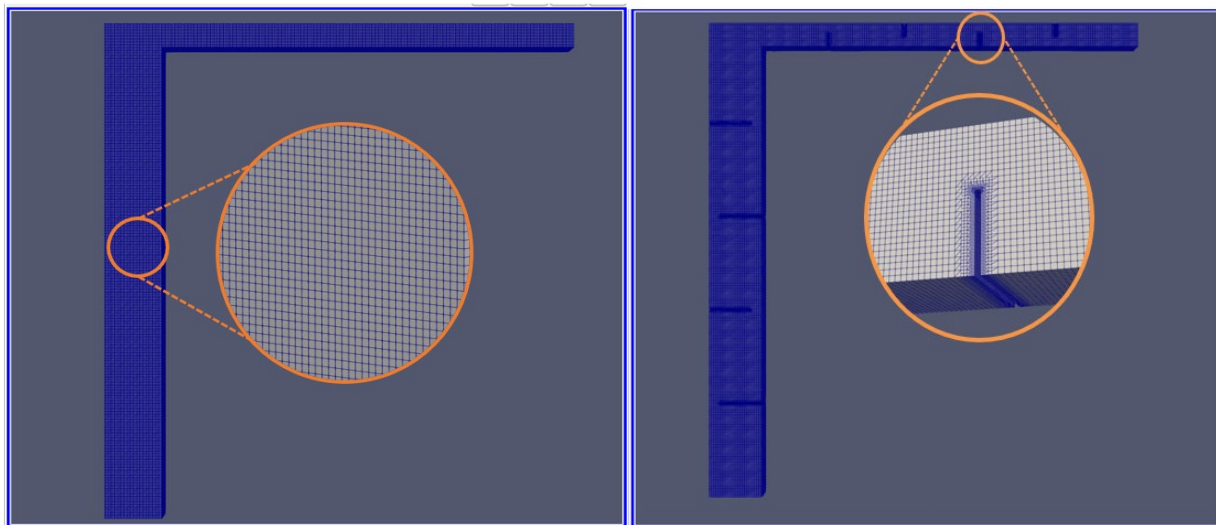


Figure 4-7. Generated mesh for channel (a) without baffle (b) with 8 baffles

For the mesh to be of good quality, it must meet some criteria such as non-orthogonality, aspect ratio, and skewness. These criteria were verified using the checkMesh command in OpenFOAM after the mesh was developed.

Furthermore, achieving mesh independence is a crucial goal in CFD simulations. It signifies that the chosen mesh is fine enough to accurately capture flow behavior and resolve important flow

features. When a simulation is mesh-independent, further refining the mesh does not significantly alter the results. This indicates that the solution has converged. For this purpose, the simulation was run with different meshes to ensure mesh independence and validation. Three created mesh for the channel with 8 baffles and for the channel with 16 baffles is shown with the number of cells in the Table 4-3.

Table 4-3. Descriptions of meshes for mesh independence assessment

	Channel with 8 baffles	Channel with 16 baffles
Mesh	Cells	Cells
Mesh 1	1 310 000	1 863 000
Mesh 2	2 496 000	3 602 000
Mesh 3	9 120 000	9 564 000

4.2.4 Configuration of OpenFOAM Numerical Model

To configure the numerical model, OpenFOAM software was employed. Among its range of solvers, the simpleFoam solver was chosen for simulating the internal flow within the hydraulic flocculator. This solver operates based on the SIMPLE (Semi-Implicit Method for Pressure Linked Equations) algorithm. Not only it is well-suited for stationary, incompressible, and single-phase flows but also it also offers stability, robust convergence, and efficiency. The solver also supports various turbulence models, allowing for the consideration of turbulent effects in the flow. As explained in the previous chapter, the standard k- ϵ turbulence model, known for its simplicity and robustness, has been selected for analyzing the flow in the hydraulic flocculator.

4.2.4.1 Solver settings

In the subsequent stages of the process using OpenFOAM software, following the user manual guidelines for implementing the k- ϵ turbulence model, three essential directories - namely, "0," "System," and "Constant" - were created. These directories store vital information for the accurate execution of the simulation, including the initial and boundary conditions. Each directory contains scripts coded in C++. For a detailed insight into the parameters and description of these directories, please refer to Appendix A.

The initial velocity is calculated for the inlet. Since the flow rate is $3.16 \text{ m}^3\text{s}^{-1}$, the velocity in the entrance is computed as 0.53 m/s . The calculated value is assigned as a constant value using the *fixedValue* condition of OpenFOAM, for all *wall-type* geometries the *noSlip* condition is given which assures the velocity of 0 ms^{-1} on that surface. The *zeroGradient* is assigned for the outlet, which means that the variable is assumed to have no variation in that surface. The flocculator outlet pressure is designated *fixedValue* with the value of 0 Pa . For the other surfaces the *zeroGradient* condition was assigned. The initial values for turbulent kinetic energy (k) and turbulent dissipation energy (ϵ) were estimated using for all *wall-type* geometries the *kwallfunction* and *epsilonwallfunction* boundary conditions was applied. These functions are designed to accurately model the near-wall behavior of turbulence. Eq 4-2 and Eq 4-3, for all *wall-type* geometries the *kwallfunction* and *epsilonwallfunction* boundary conditions was applied. These functions are designed to accurately model the near-wall behavior of turbulence.

$$k = \frac{3}{2} (I |U_{ref}|)^2 \quad \text{Eq 4-2}$$

$$\epsilon = \frac{C_\mu^{0,75} k^{1,5}}{L} \quad \text{Eq 4-3}$$

In this equation, I represents turbulence intensity which was considered as 10%, C_μ is a constant with value of 0.09 and L^1 is defined as turbulence length scale (P. Melo, Freire, Ansoni, Oliveira,

¹ $L = 0.07 \times l$

& Franco, 2022) Calculated and assumed values are presented in Table 4-1. In addition, there is two file names *fvScheme* and *fvSolution* which should be revised according to the simulation conditions. These files are crucial in setting up a CFD simulation, *fvSolution* in OpenFOAM sets parameters for linear equation solvers, including solver type, convergence tolerances, and relaxation factors for variables. Moreover, *fvSchemes* defines numerical discretization schemes for variables, determining how gradients and Laplacians are calculated in the discretized equations.

Table 4-4. Calculated parameters for turbulence model

parameter	symbol	unit	value
Hydraulic diameter	l	m	2.44
Kinematic viscosity	ν	m^2s^{-1}	1×10^{-6}
Velocity	V	ms^{-1}	0.53
Reynolds number	Re	-	1.3×10^6
Turbulence intensity	I	%	10
Turbulence length scale	L	m	0.17
turbulent kinetic energy	k	m^2s^{-2}	42.135
turbulent dissipation energy	ε	m^2s^{-3}	108.088

Shaw (1992) introduced a simplified flowchart which is shown in the Figure 4-8. The flowchart serves as guiding roadmap through the process of Computational fluid dynamics from problem thinking to the result analysis. Moreover, there are more detailed steps not covered in this chart, including boundary conditions and the selection of a turbulence model.

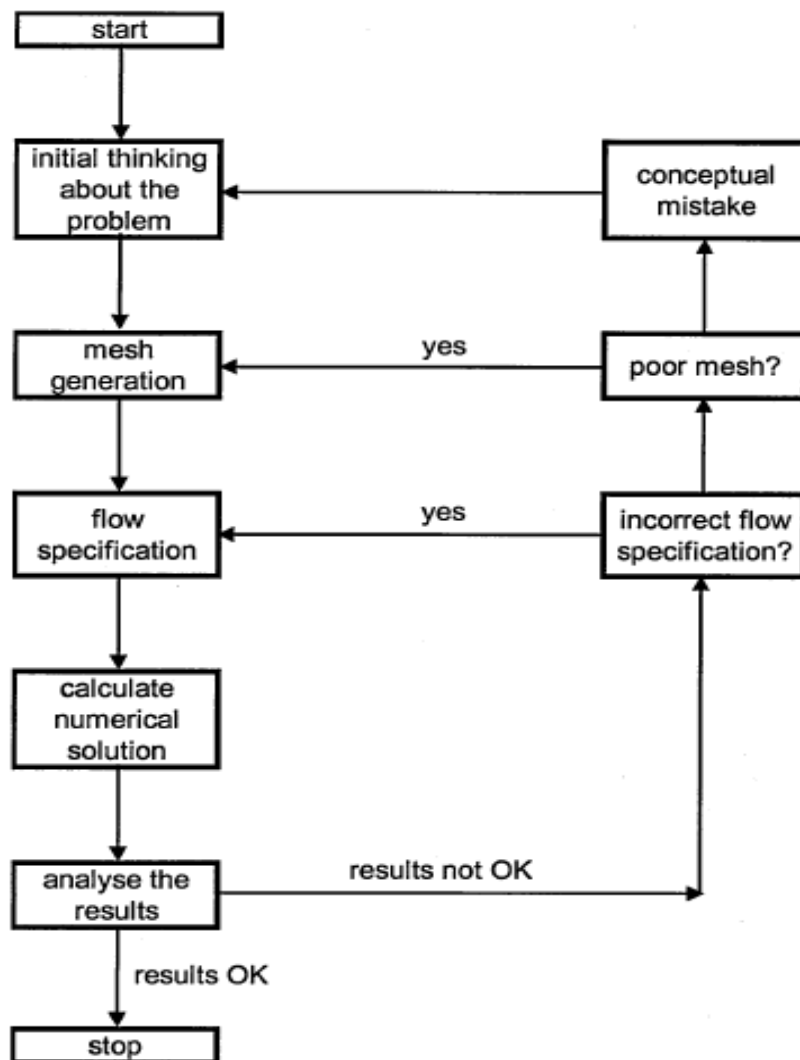


Figure 4-8. The CFD analysis process (Shaw, 1992)

4.2.4.2 Computational Resources

The computational simulations were performed utilizing the resources provided by Compute Canada, specifically the Cedar cluster. Compute Canada is a cloud national platform that offers researchers access to high-performance computing (HPC) infrastructure. The Cedar cluster, with its advanced processing capabilities and plentiful memory resources, was employed for this project. Figure 4-9 depicts the Compute Canada chart detailing the steps for running a simulation on the Cedar cluster.

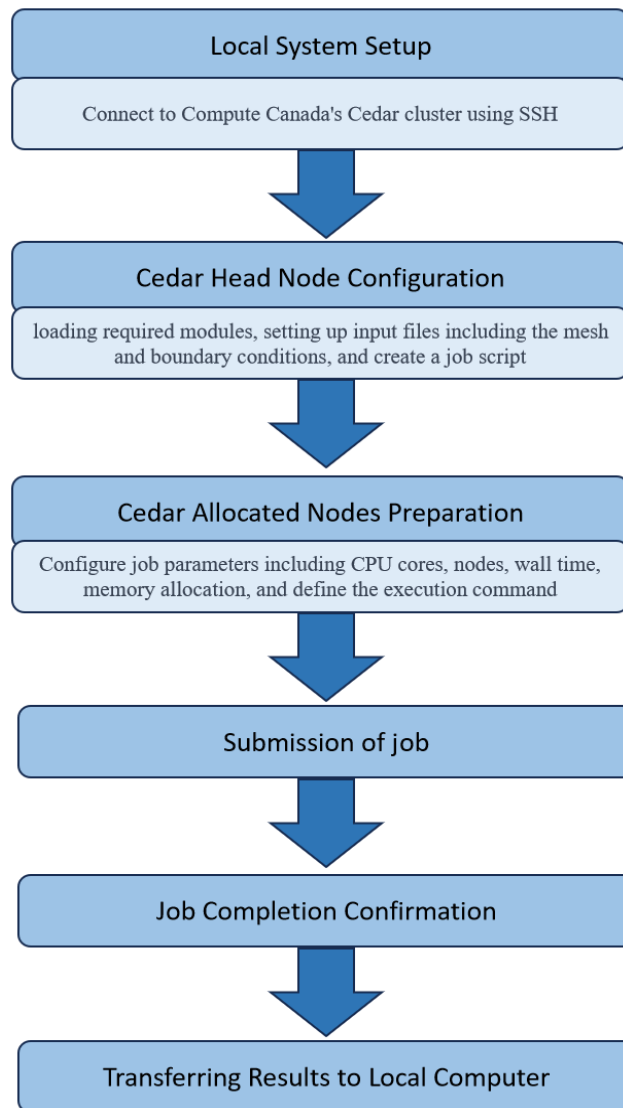


Figure 4-9. Compute Canada Chart for Running a Simulation on Cedar Cluster

4.3 Experimental studies

4.3.1 Overview of experimental protocol

The objective of this experiment is to obtain the floc growth kinetics at the DesBaillet water treatment plant in order to integrate it within the CFD model. The raw water was collected from the intake of the Des Baillet plant, sourced from the St. Lawrence River. Sampling was carried

out in October, although the Dissolved Organic Carbon (DOC) levels were not at the desired peak condition (3.5- 4 mg C/L). To address this issue, the Des Bailleurs water was combined with more turbid water from the Des Prairie River, allowing us to achieve the target peak season DOC for our tests. Specifics regarding the characteristics of each water sample, as well as the final combined water, can be found in Table 4-5.

Table 4-5. Water characteristics

Raw Water	pH	Alkalinity	Turbidity	TOC	DOC
		mg CaCO ₃ /L	NTU	mg C/L	mg C/L
DesBailleurs	7.86	71	1.63	2.82	2.72
DesPrairies	6.56	23	10.65	7.28	7.08
DesBailleurs (85%) + DesPrairies (15%)	7.81	56	3.66	3.82	3.4

The test consists in carrying out a *Jar Test* and then analyzing the samples to measure flocs diameter. The experiment commenced with a jar test, as PAX-XL 1900 (Aluminum Chlorohydrate) which is already in use at the plant. Since the selected coagulant is highly pre-hydrolyzed (82%), it cannot be diluted significantly. A series of tests were conducted under the following specified parameters:

- Temperature: 22°C
- Coagulant type: Aluminum Chlorohydrate (PAX-XL 1900)
- Coagulant dosage: 0.5 to 2 mg Al/L
- Flash mix intensity: $G = 100 \text{ s}^{-1}$
- Slow mix intensity: $G = 50 \text{ s}^{-1}$
- Mixing time: 5, 10, 15 minutes

The Jar tests (shown in **Error! Reference source not found.**) were initiated with rapid mixing at $G=100\text{ s}^{-1}$ (99 rpm) while introducing the coagulant (0.5 to 2 mg Al/L), the flash mix continued for up to 1 min to rapidly disperse coagulants into the water to ensure uniform distribution. Subsequently, the slow mix with $G=50\text{ s}^{-1}$ (56 rpm) began for required time of 5, 10, or 15 minutes. This encourages the already-formed flocs to collide and adhere to each other, creating even larger and denser flocs. The summary of the test protocol is shown in the Table 4-6.



Figure 4-10. Jar-test

Table 4-6. Jar-test protocol

Jar-test protocol
Flash mix: 1 min in 100 s^{-1}
Slow mix: 5,10,15 min in 50 s^{-1}

4.3.2 Measurement of floc growth kinetics

One of the objectives of this study is to measure the flocs size and consequently predict a flocs growth kinetics for the Des Baillet water treatment plant. In direct filtration due to the absence of sedimentation step, it is aimed to form flocs between 10 to 50 microns rather than larger settleable flocs (MELCC 2019), so this is the range that we anticipate our flocs to be. In this stage of the project, three different methods of flocs analysis were employed: Laser Diffraction particle analyzer, Direct Photometric Analyzer, and direct microscopy.

4.3.2.1 Laser Diffraction Particle Analyzer (Mastersizer 3000)

Mastersizer 3000 is a particle size analyzer designed by Malvern Instruments, a company that specializes in particle size analysis and characterization. It uses a laser diffraction technique to measure the size distribution of particles in a sample. In this instrument, a laser beam is used to shine through a dispersed sample to measure the particle size distribution from 0.1 μm to 3 mm.

When particles scatter light, the scattering pattern provides information about how large the particles are. The smaller particles scatter light at higher angles and on the contrary bigger particles scatter light at lower angles.

The Mastersizer 3000, depicted in Figure 4-11, is widely used in pharmaceuticals, food processing, ceramics, chemicals, and environmental sciences, among others, where accurate knowledge of particle size distribution is essential.



Figure 4-11. Mastersizer 3000

The *Mastersizer Software* needs us to fill out information related to our samples, such as particle shape, material, density of solvent, estimation of particle size for more accurate measurements. In our samples the particles were considered non-spherical, aluminum base material with particle range of 10 to 1000 μm . Each time before commencing the test, we conducted an *Initialization* and *Background Measurement* using clean water to ensure that everything was in proper order and ready for particle measurement. After stirring the sample with the jar test, due to the possibility of floc settling and the importance of contact time, we promptly transferred 300 ml of the sample into a standard beaker and initiated the device. To facilitate the solution transfer, a

pump is connected to a tubing system, which transfers the solution from the beaker to the measurement chamber. Furthermore, the diameter of the equivalent sphere was directly obtained from the particle measurements. For every 10 consecutive measurements, the system generated a comprehensive report on the particle size distribution range including average and variance of particle diameter as well as Dv10, Dv50, and Dv90. We have duplicated the measurement tests to evaluate the precision of the results.

4.3.2.2 Direct Photometric Analyzer (Brightwell)

Brightwell Technologies INC's DPA 4100 Flow Microscope is a specialized instrument used for particle analysis in range of 2 to 300 μm . It combines the features of a Direct Photometric Analyzer (DPA) with flow microscopy technology. Brightwell analyzes particles in a liquid sample by measuring their size, shape, concentration, and other characteristics. As shown in Figure 4-12, a *Flow Cell* allows continuous imaging of particles in motion in contrast to traditional microscopy, which examines samples on static slides. *Flow Cells* are used to capture the image of particles in real time as they pass through them. It has software for collecting and analyzing data, allowing for the capturing, and processing of images and measurements. There are several applications for this instrument, including environmental monitoring, pharmaceuticals, industrial quality control, water treatment, and research that require detailed particle characterization.

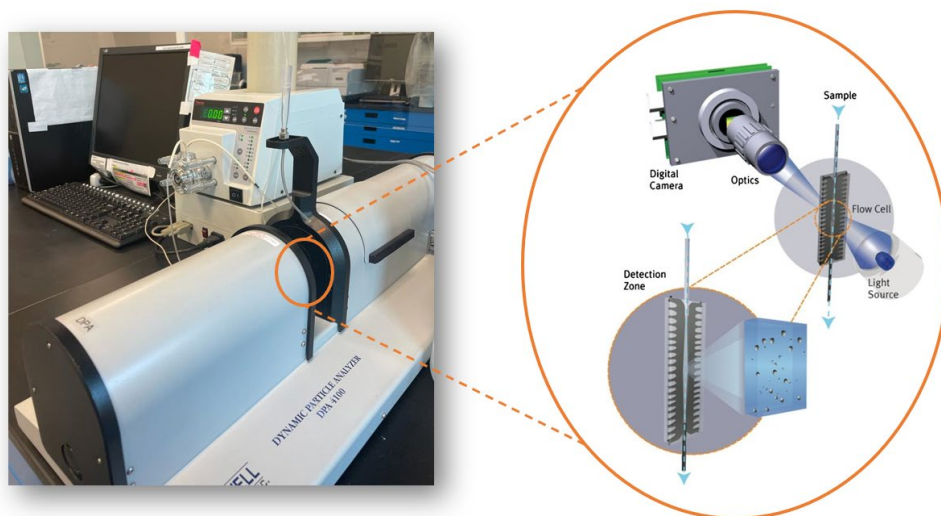


Figure 4-12. Brightwell Technologies INC's DPA 4100

To initiate the process, the chosen *Flow Cell* should be cleaned thoroughly with a mixture of water and detergent, followed by rinsing with Mili-Q water and a final wipe-down with isopropanol. Once the *Flow Cell* is correctly installed, each cell requires specific configuration settings based on its model, along with precise focus adjustment. The following stage passes the Mili-Q water for 2 minutes to ensure the cleanness of tubes and cells.

Prior to each sample analysis, the *Optimize Illumination* is performed in order to obtain accurate and reliable results. The device is prepared for sample measurement, the samples were carefully pipetted from the Jartester to prevent any disruption of formed flocs and transferred to the 1 ml pipette tip positioned above the *Flow Cell*. Moreover, the samples were extracted directly from a pipette tip through the *Flow Cell*, utilizing a peristaltic pump with a flow rate of 0.23 ml/min. The measurement of particles occurred while the sample passed through the *Flow Cell*. Finally, the instrument's software captured and recorded images and data from the *Flow Cell* microscope, as well as generated targeted reports. The overall protocol of sample measurement using Brightwell is illustrated in Figure 4-13.

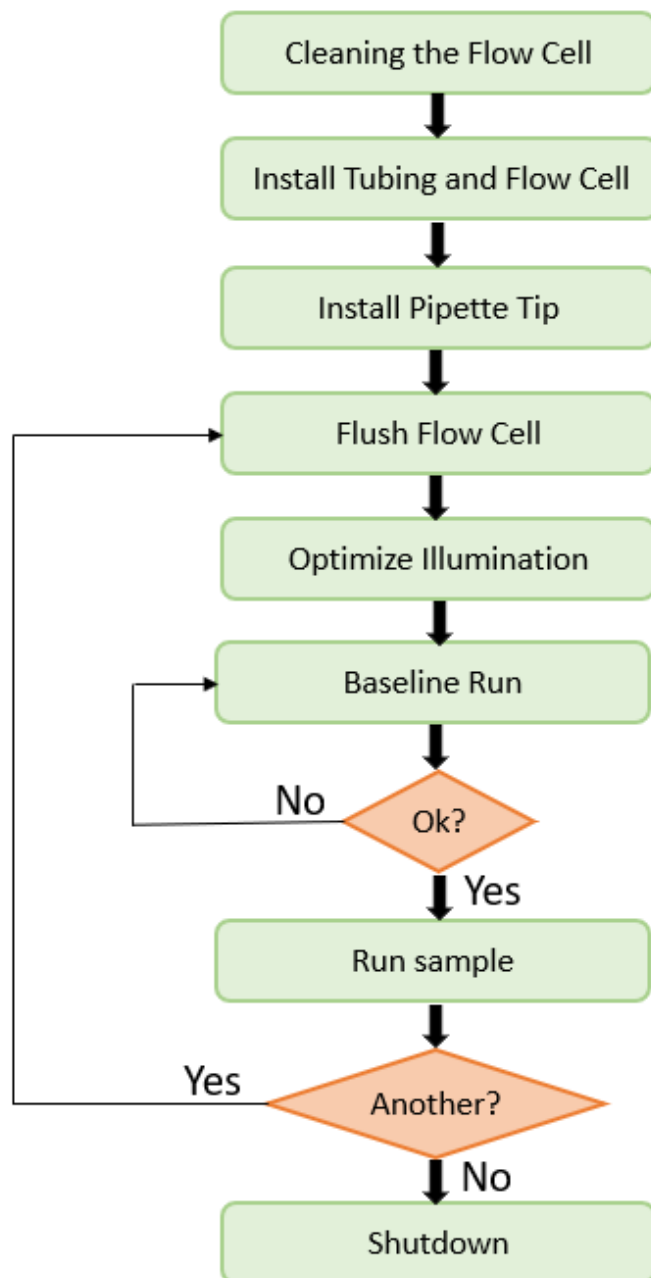


Figure 4-13. Protocol of sample measuring with Brightwell technology (DPA 4100)

4.3.2.3 Microscopy

For this project, since the flocs could not be measured successfully using the Laser Diffraction particle analyzer and Direct Photometric Analyzer, the microscope was employed as a third option. The Olympus BX51 microscope is a versatile and widely used research-grade microscope

known for its high-quality optics and advanced imaging capabilities, shown in the Figure 4-14. It employs various lenses and prisms to manipulate and magnify light passing through the sample, range of objective lenses with different magnification levels and numerical apertures, allowing for detailed examination of specimens at varying levels of magnification.



Figure 4-14. Olympus BX51 microscope

To start the Olympus BX51 microscope, the following steps took place: first the desired objective lens (10X) was chosen,. Next, the illumination was adjusted and the samples was pipetted directly from the Jartester in a 10 ml bottle. The locs were then stained for better visualization under the microscope using *Methylene Blue* at a 0.1% (v/v) ratio which was gently added to the sample to prevent the floc breakage. Following this, 1 ml of sample was taken using a clean pipette and carefully placed on the 1.0 mL Gridded Sedgewick-Rafter Counting Cell. An Olympus DP70 camera (100X) linked to the microscope was used to capture the images. For each sample, 10 images were taken from different locations of the cell. Below is an example of captured images employing the microscope for the sample with 2mg Al/L of coagulant and 5 min of slow mix in the Figure 4-15.

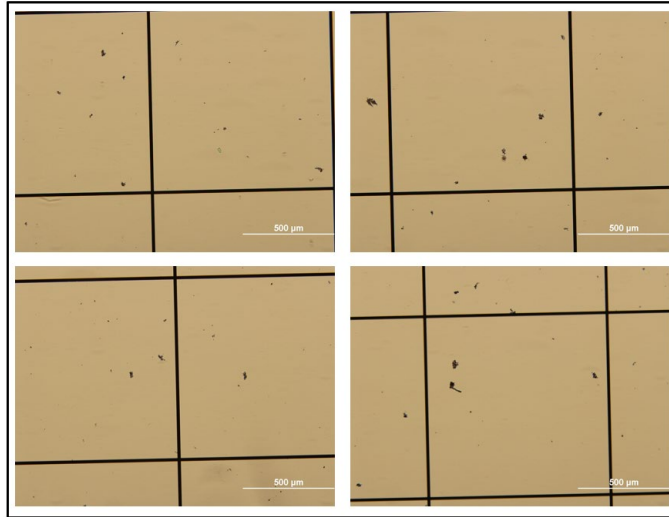


Figure 4-15. Captured images using microscopy

Subsequently to measure the flocs size, the image was analyzed employing the ImageJ processing software with a calibrated scale (ImageJ, 2005). All the observed flocs in the images were encircled using an elliptical shape. Using the measurement option, the software generates a report containing the area and perimeter of each ellipse. With this information, the diameter and average volume diameter of the flocs for each sample was computed.

CHAPTER 5 Results and Discussion

In this chapter, we present the findings from both the numerical (CFD) simulation and the experimental study. We begin by discussing the outcomes of the CFD model, followed by an analysis of the results from our experimental work. Finally, we integrate the experimental results into the CFD analysis.

5.1 CFD Model Application

The CFD model was carefully designed to evaluate the flow patterns within the hydraulic flocculator, enabling precise calculations of dissipation energy rate, velocity gradient, residence time, and head loss in the channel. This important step gave us valuable knowledge about how the system behaves, helping us understand how well the flocculation and hydraulic processes work.

5.1.1 Model Convergence

5.1.1.1 Mesh Independency test

Reaching mesh independence is vital in CFD simulations. This means that the selected mesh is fine enough to precisely capture how the flow behaves and identify important flow characteristics. When a simulation is mesh independent, making the mesh even finer doesn't change the results much. This shows that the solution has converged effectively. In this study, the mesh analysis took place using the Grid Convergence Index (GCI) Method to check the accuracy of three different meshes. The velocity in specific lines (Figure 5-1) in the flocculator with 8 baffles for each mesh is illustrated in Figure 5-2 and Eq 5-1 is employed to calculate the GCI accordingly.

$$\begin{aligned}
 GCI &= F_s \frac{e_{rms}}{r^2 - 1} \\
 e_{rms} &= \sqrt{\frac{\sum_{m=1}^{1000} |(u_{m,1} - u_{m,2}) / u_{m,2}|^2}{1000}} \\
 r &= \left(\frac{h_2}{h_1}\right)^{1/3}
 \end{aligned}
 \tag{Eq 5-1}$$

Where, u_m Represents the velocity magnitude in meshes 1 and 2, h is depicting the number of cells in each mesh, where mesh 1 and 2 represent coarser and finer mesh accordingly.

The F_s Is the factor of safety that multiplies the relative error. Based on previous works, a value of 1.25 is selected for this study. (Schwer, 2008)

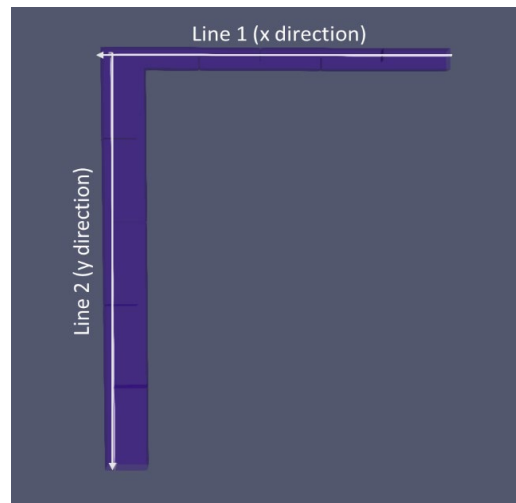


Figure 5-1. Specified lines in the flocculator geometry for mesh convergence analysis

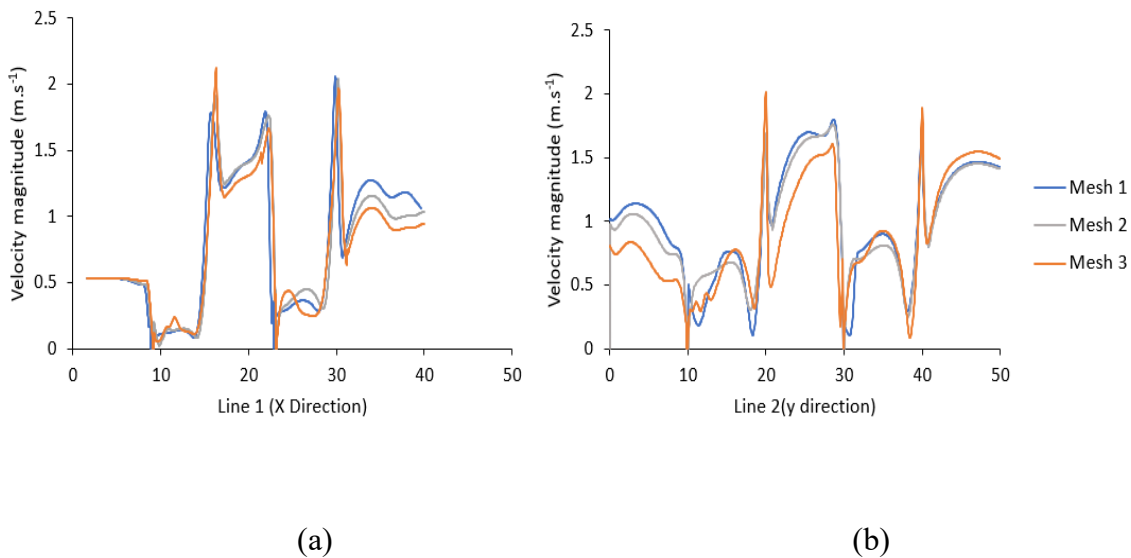


Figure 5-2. Mesh quality influence over the magnitude of velocity over (a) line 1 and (b) line 2

Table 5-1. Convergence test results

Mesh	Channel with 8 baffles		Channel with 16 baffles	
	Cells	GCI	Cells	GCI
Mesh 1	1,310,000	13%	1,863,000	11%
Mesh 2	2,496,000	5.4%	3,602,000	6.7%
Mesh 3	9,120,000	-	9,564,000	-

As depicted in **Error! Reference source not found.**, the Grid Convergence Index (GCI) for Mesh 1 compared to Mesh 2 is 13%, while for Mesh 2 compared to Mesh 3, it is 5.4%. Given that mesh 2, with GCI of 5.4%, offers an accurate representation of the fluid, and considering that Mesh 3 requires nearly three times the computational time of mesh 2, mesh 2 was selected for the simulations. A similar assessment was conducted for the channel with 16 baffles, and the mesh 2, with 3,602,000 cells, was selected due to the acceptable GCI of 6.7%.

5.1.1.2 Residuals

Residuals represent variations in values between iterations. At every stage of the process, alterations in parameters such as velocity, k , and epsilon occur at grid points. These differences between the current values and those from the prior step are labeled as residuals. Visual representations of these differences are presented in a graph, allowing us to observe how the magnitude of residuals evolves with each additional step. The results are considered converged when these differences become small enough that the solution can be considered sufficiently accurate. The considered value as convergence criteria in this study is 10^{-3} . The residual graphs for the channel with 8 and 16 baffles are demonstrated in Figure 5-3 and Figure 5-4. The residuals in both cases exhibit a decreasing trend, signifying that a satisfactory level of accuracy is reached, and the results can be considered reliable for further analysis or application.

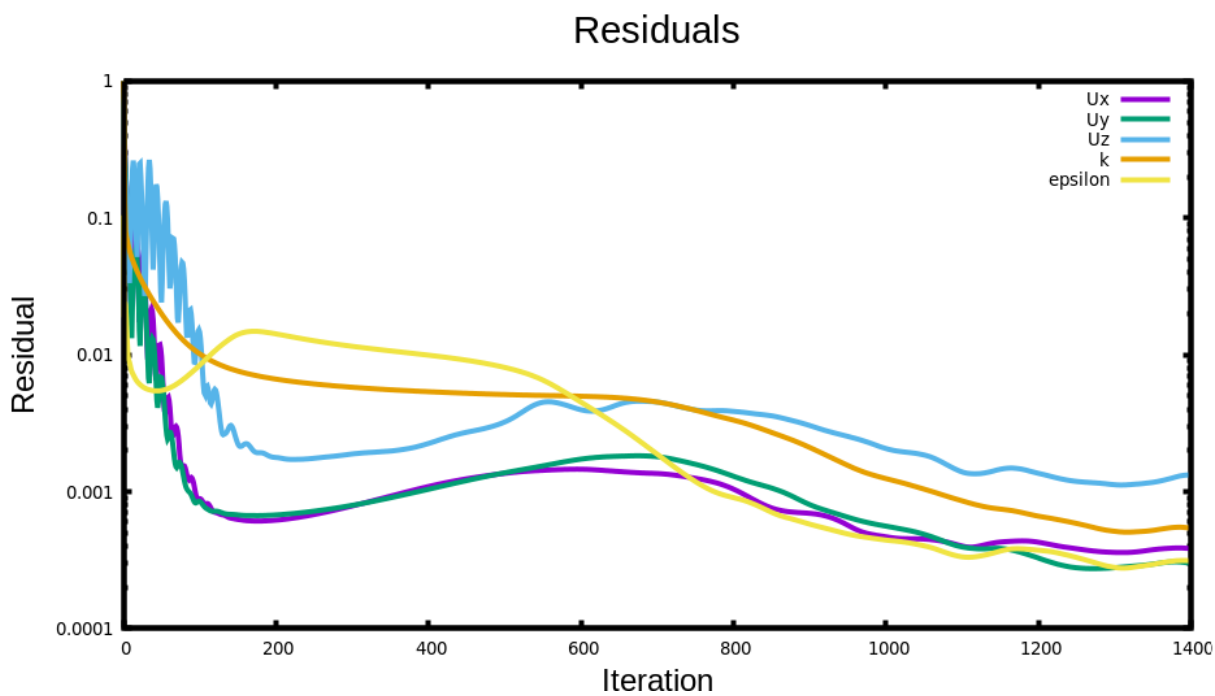


Figure 5-3. Residuals of CFD simulation for the channel with 8 baffles

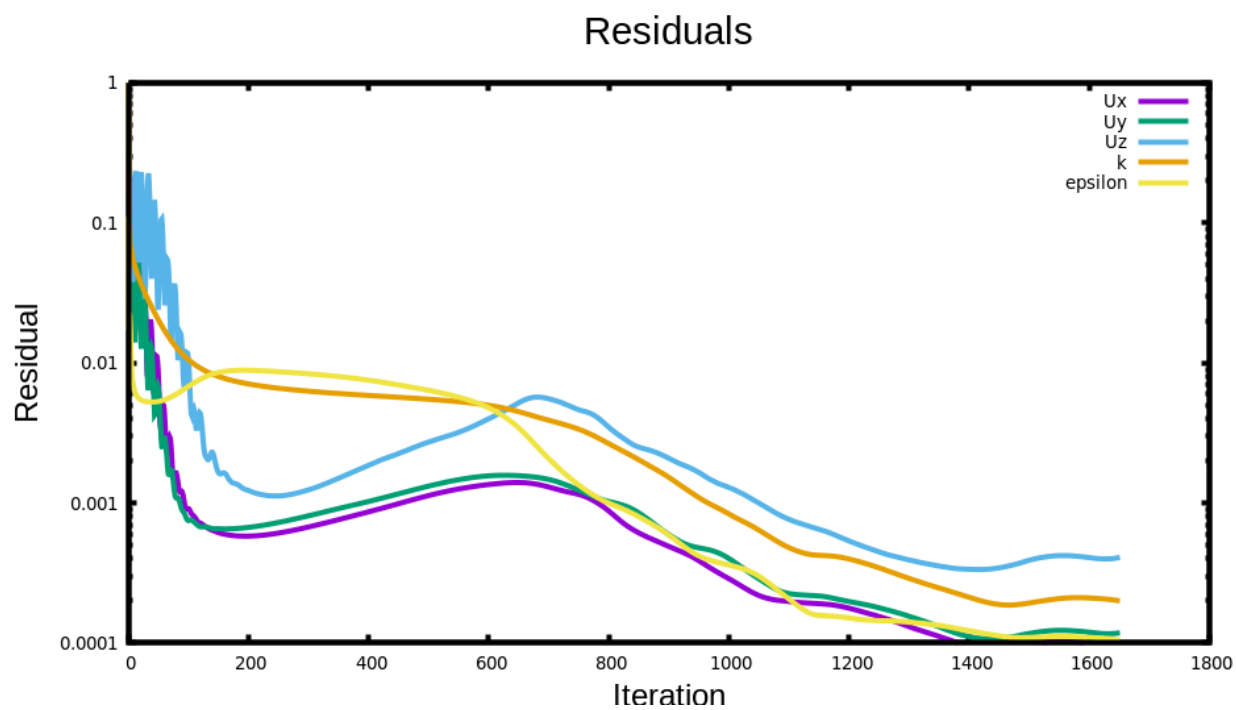


Figure 5-4. Residuals of CFD simulation for the channel with 16 baffles

5.1.2 Velocity Field Analysis

The velocity streamline could be obtained as a result within the OpenFOAM software and visualized using the Paraview. Figure 5-5, displays velocity distributions in channels equipped with 8 or 16 baffles. Difference in the flow pattern of channels is observed and demonstrated that recirculation region length is influenced by the number of baffles as demonstrated by Saha et al. (2021). The inlet velocity for each case was 0.53 m.s^{-1} . In the channel with 8 baffles 50% of the velocities range between 0.15 ms^{-1} and 0.73 ms^{-1} , while in the channel with 16 baffles, 50% of the velocities fall between 0.8 ms^{-1} and 1.3 ms^{-1} . Furthermore, the velocity in the channel with 8 baffles peaks at 2.2 ms^{-1} , approximately 3.77 times higher than the inlet velocity while in the channel with 16 baffles, the velocity reaches 1.6 m.s^{-1} , which is 3.01 times higher than the inlet velocity. The calculated values are in accordance with the result of Saha et al. (2021) study on the velocity behavior in the flocculator with different configurations of baffles. This information suggests a more consistent velocity pattern in the 16-baffle channel, which indicates a smoother and controlled flow regime. This contrasts with the 8-baffle channel, where there is a noticeable and abrupt change in velocity. The rapid velocity transition in the 8-baffle channel may lead to a higher shear rate which could affect the overall flocculation efficiency.

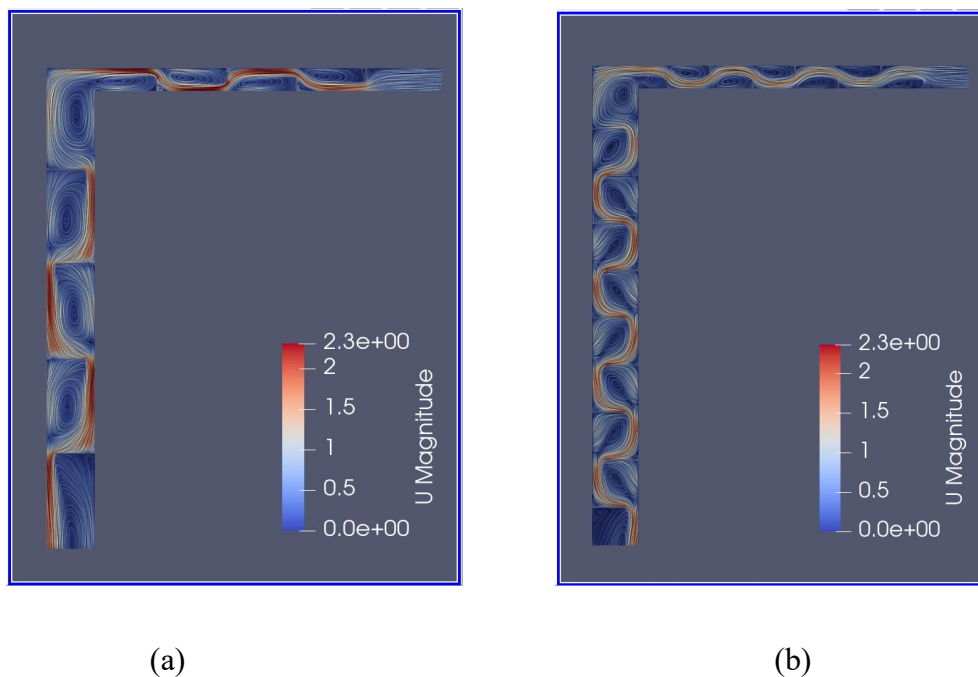


Figure 5-5. Velocity profiles (in m.s^{-1}) in the flocculator with (a) 8 baffles and (b) 16 baffles

5.1.3 Turbulent dissipation energy (ϵ)

Figure 5-6 displays (2D) epsilon values obtained from the K-epsilon model for channels both with and without baffles. In the channel without baffles, the dissipation rate is generally low, with the only notable dissipation occurring at the corner of the channel. However, upon the introduction of baffles, a significant increase in energy dissipation becomes evident. As anticipated, the edges of the baffles exhibit the highest levels of energy dissipation. When comparing channels with 8 and 16 baffles, it becomes evident that the intensity of energy dissipation along the baffle edges is lower in the channel with 16 baffles. Conversely, between the baffles, a greater amount of energy dissipation occurs. The dispersion of turbulent dissipation energy in channels with 8 baffles and 16 baffles is also illustrated in Figure 5-7 for more evident comparison (the channel without a baffle has been excluded from the graph due to its very low values of epsilon). In depicted whisker plot, the central box represents the interquartile which spans from the 25th percentile to the 75th percentile of data, containing 50% of data, the upper whisker extends to the maximum value above the 75th percentile and the lower whisker extends to the minimum value below the 25th percentile. Based on this analysis, the dissipation energy values range from 0.01 to 0.15 $\text{m}^2 \cdot \text{s}^{-3}$ for 16 baffles in the channel and the mean is situated inside the 50% box. In contrast, the 8-baffle configuration exhibits higher variability, with observed values ranging from 0.01 to 0.25 and the mean being located on the upper and outside of the box indicating there are some relatively high values that are pulling the mean upward.

This suggests that the 16-baffle configuration may lead to more reliable and stable performance in the hydraulic flocculation process compared to the 8-baffle configuration. The channel with 16 baffles seems to contribute to a more equal dispersion of the observed values, indicating a potentially more controlled and consistent process.

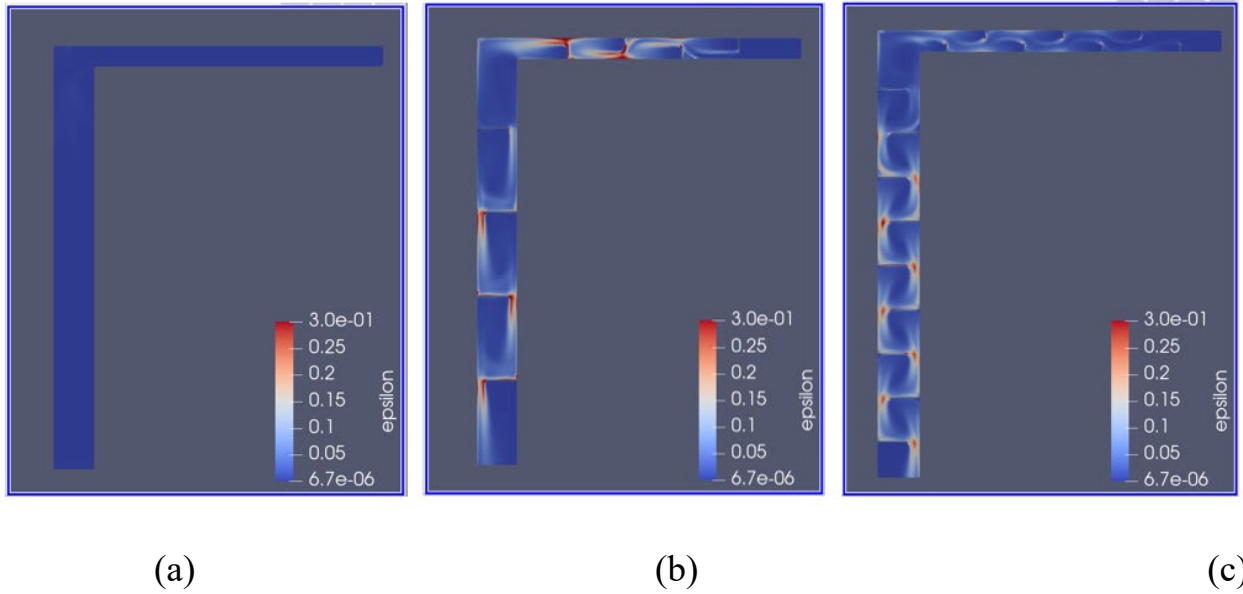


Figure 5-6. Epsilon variation (in $\text{m}^2.\text{s}^{-3}$) in the flocculator (a) without baffle (b) with 8 baffles (c) with 16 baffles

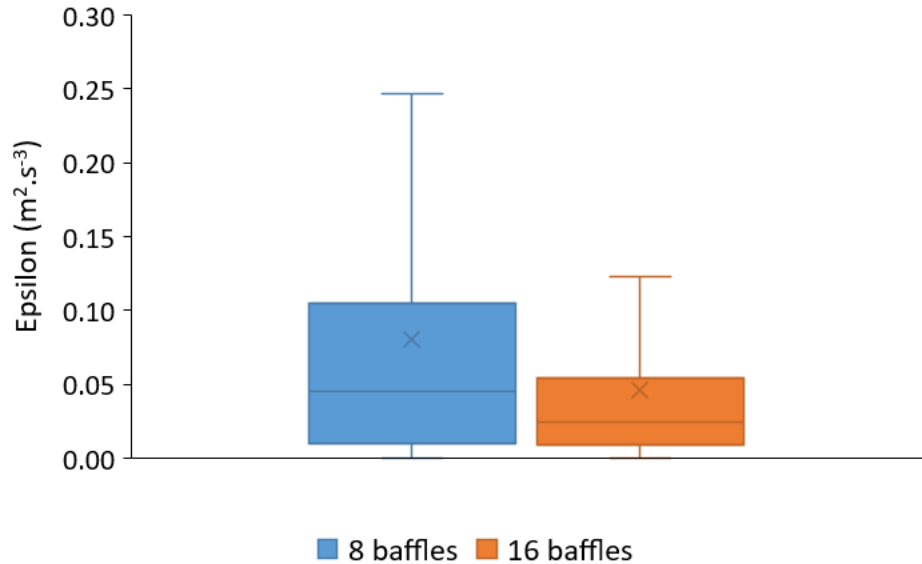


Figure 5-7. Epsilon distribution in the channel with 8 and 16 baffles

Notably, one of the primary objectives in designing a flocculator is to intentionally create head loss in the channel. Head loss includes all the stresses caused by a disturbance in the flow. It can

be a change of direction in the bends or a change of section because of the baffles, narrowing, or a widening (Kawamura, 2000).

John Bridgeman and colleagues (2010) study on the flocculator design illustrates that the introduction of baffles leads to an increase in hydraulic head loss, thereby enhancing flocculation. As depicted in Figure 5-6, there is a notable elevation of dissipation energy in the channel with baffles compared to the one without baffles. Observation serves as evidence of the intentional generation of head loss within the channel. The calculated major head loss from CFD for the channel with 8 baffle is 1.21 m and for the channel with 16 baffles is 1.27 m. It is worth noting that, as presented in the Table 5-2, the calculated head loss obtained from CFD simulation results is much higher than the target head loss determined using the minor head loss equation. (Depicted in the Table 4-2. Baffles design parameters).

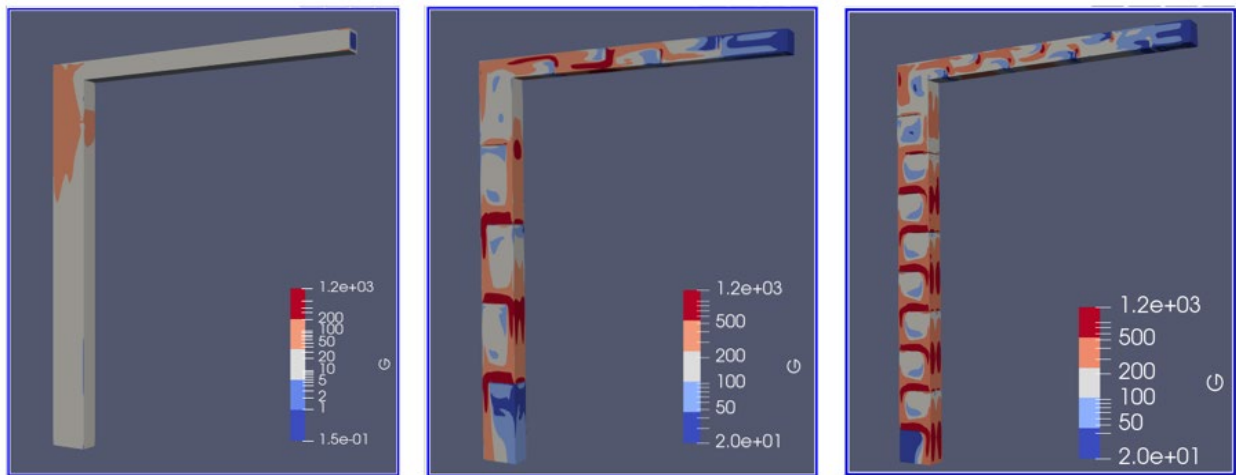
Table 5-2. Head loss comparison from simulation and target head loss

	Head loss from simulations (m)	Target head loss (m)
Channel with 8 baffles	1.21	0.75
Channel with 16 baffles	1.27	0.75

5.1.4 Velocity Gradient (G value)

The extracted epsilon value is used in the gradient velocity equation to obtain the G value in each cell through the whole mesh. Therefore, we were able to conduct a numerical assessment of how turbulence behaved within the structure. Given the significance of analyzing the velocity gradient values for the flocculation process, it is crucial to examine how these parameter changes in a fluid as it moves through. The variation of G value in the channel with 8 and 16 baffles and the channel without baffles is shown in Figure 5-8 for comparison in a logarithmic scale in 3D view. As it is shown, for the channel without baffle the velocity gradient is not noticeable and the

maximum amount occurs in the corner of the channel, where the dissipation energy happened, with the value of 60 s^{-1} . After adding the baffles, the G value exhibited significant variation through the channel. The velocity gradient value was found to be higher, towards the edges of the baffles and on the walls opposite, which completely aligns with the results of John Bridgeman et al. (2010).



(a)

(b)

(c)

Figure 5-8. G value in the flocculator (a) without baffle (b) with 8 baffles (c) with 16 baffles

The analysis of cumulative frequency distribution shown in Figure 5-9, as described in previous studies (Bridgeman, 2010; Vadasarukkai, 2011), enables us to compare G values distribution in the cases examined in this study. For instance, for the channel without baffle 70 percent of the total channel has a range of G values lower than 60 s^{-1} , whereas the maximum value is smaller than 100 s^{-1} . Going forward, the graph for 8 baffles illustrates the wide range of G value spanning from 10 s^{-1} to over 1000 s^{-1} . Meanwhile, the channel with 16 baffles the G value range of up to 500 s^{-1} , and nearly half of them fall in the range of 100 s^{-1} to 220 s^{-1} . It seems that the presence and number of baffles significantly influences the flow characteristics in the channel (Joodi, 2013). Specifically, the channel with 16 baffles leads to less variation of G value through the channel and more controlled and constrained flow. An improvement in the turbulence condition is seen, which ensures smoother mixing rate and preservation of formed flocs (P. Melo et al., 2022). In summary, a channel with controlled flow can promote more effective flocculation by

providing an environment where flocs can grow and develop without being overly subjected to disruptive shear forces.

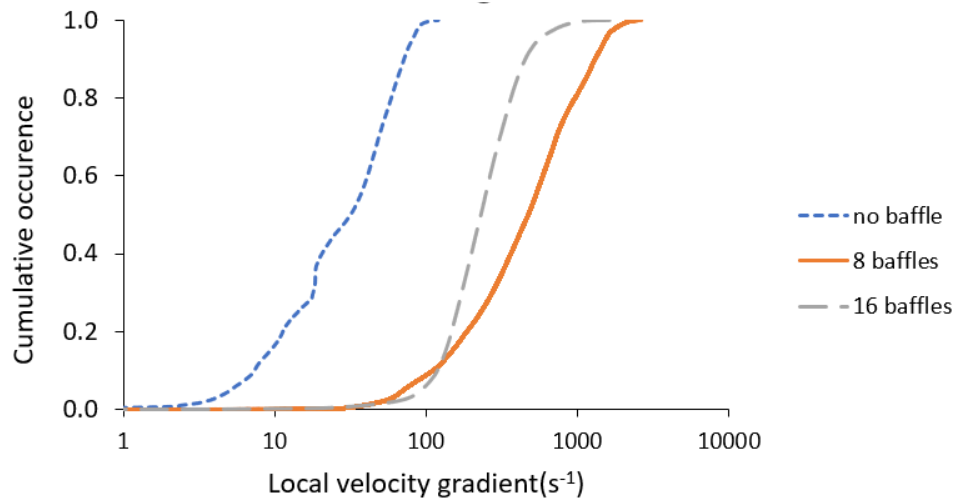


Figure 5-9. Cumulative frequency distribution of G value in the channel without and with baffle

5.1.5 Camp number (Gt)

Camp and Stein's work in 1943 on velocity gradients, led to the development of the Camp number (Gt) which is the product of the mixing intensity and time (Gt). One way to qualitatively evaluate the design conditions of flocculators is by using the Camp Number. Figure 5-10 shows visual representations of the Camp number for the channels without and with baffles for a side-by-side comparison. In this Figure, the increase of Gt is clear in our results after adding the baffles.

The channel with baffles begins with a lower Gt at the entrance and rises until the exit of the flocculator, the change of Gt in the channel with 16 baffles happens more steadily than the channel with 8 baffles. Additionally, it is noteworthy that in certain areas, recirculation leads to higher Gt values because of higher residence time. The observation of Gt suggests that the channel with 16 baffles has a greater proportion of its area experiencing higher Gt values compared to the channel with 8 baffles. As mentioned in the previous section regarding the local

G values, the 16-baffle configuration likely provides a more uniform and stable mixing effect throughout a larger portion of the channel. This can be advantageous in processes where achieving a consistent and thorough mixing of substances or particles is crucial.

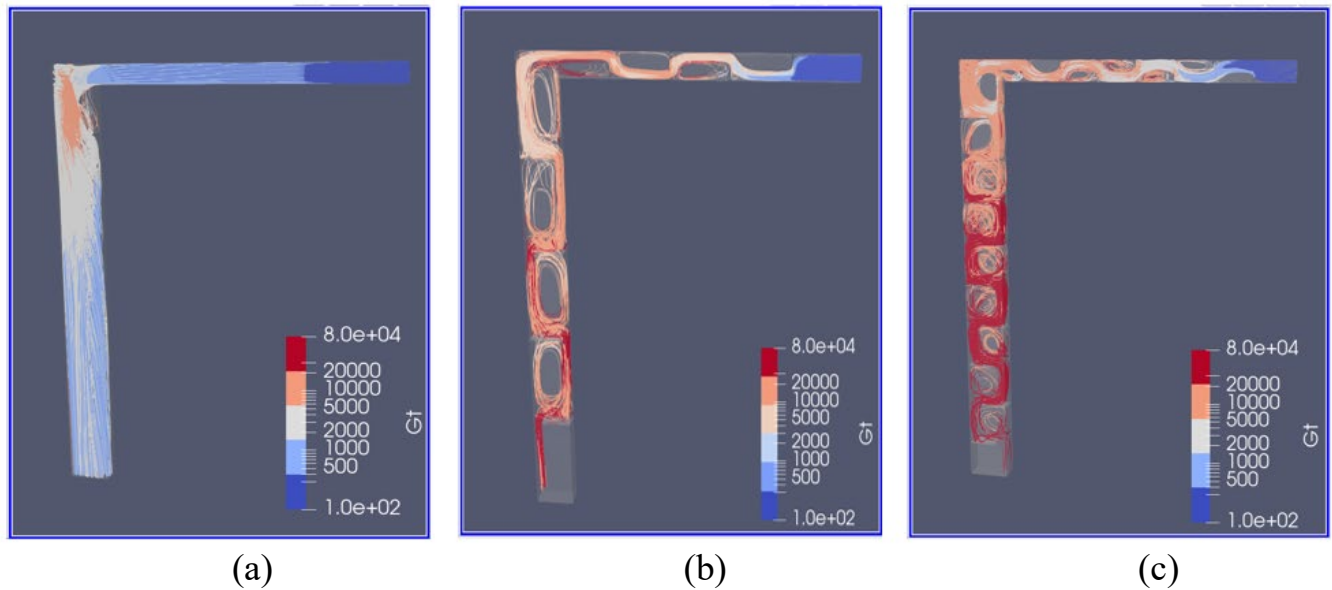


Figure 5-10. Gt value in the flocculator (a) without baffle (b) with 8 baffles (c) with 16 baffles

The Gt value at the end of the flocculator where the water enters the filters holds significant importance in the design, as this value influences the flow into the filters and provides insights into the floc diameter. In this section, computed Gt values are presented in Figure 5-11 for the flow at the flocculator outlet, both before and after the introduction of baffles. Upon introducing 8 baffles, observations in the channel show that 50% of the Gt data at the exit of the flocculator varies between 16,000 and 36,000, with a mean value of 26,000. Furthermore, in the outlet of the flocculator with 16 baffles, 50% of the data range between 45,000 to 60,000, with a mean value of 53,000. Recall that, the recommended Gt for is ranging from 3×10^4 to 2×10^5 . (Kawamura, 2000)

These findings demonstrate a significant improvement in the performance of the flocculator with the introduction of baffles, particularly in the configuration with 16 baffles, where a higher mean value and reduced variability in Gt data suggest enhanced efficiency in flocculation.

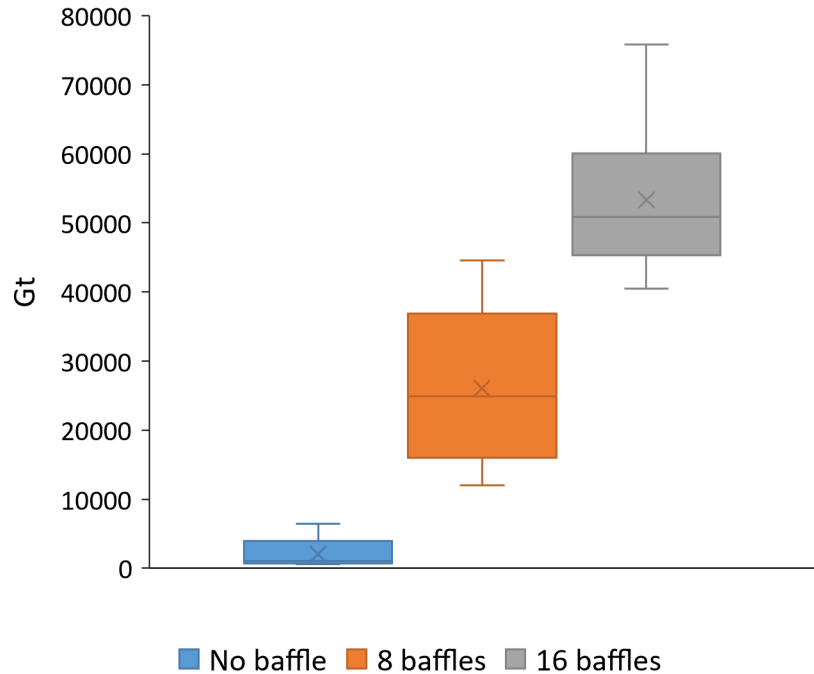


Figure 5-11. Gt values at the exit of the flocculator in the channel without and with baffle

5.2 Floc kinetic experimental measurement

One of the primary objectives of this study is to measure the flocs size and consequently achieve a flocs growth kinetics for the Charles-J. Des Baillet water treatment plant. The floc measurements take place after the jar test procedure. The results obtained from the three employed methods for floc measurement are presented below.

5.2.1 Laser diffraction Particle analyzer (Mastersizer 3000)

The initial test was conducted using the Mastersizer 3000, with the test procedure outlined in Table 5-3. This test was replicated four times using the same water batch, showing significant variations in floc sizes. The findings of two series are graphically represented in Figure 5-12. As depicted, the volume average diameter was computed for each sample under varying coagulant dosages and mixing durations. Test 1 results indicate floc diameters within the 10-100 μm range,

while Test 2 reveals floc sizes ranging from 100-1000 μm . Given the contradicting results, it raises questions about the reliability of this method for accurate floc size determination.

Table 5-3. Mastersizer 3000 test protocol

Test Protocol
PAX-XL 1900: 0.5 – 0.9 mg Al/L
Mixing intensity: 50 rpm
Mixing time: 5 to 15 min
Raw Water DOC: 3.5 mg C/L

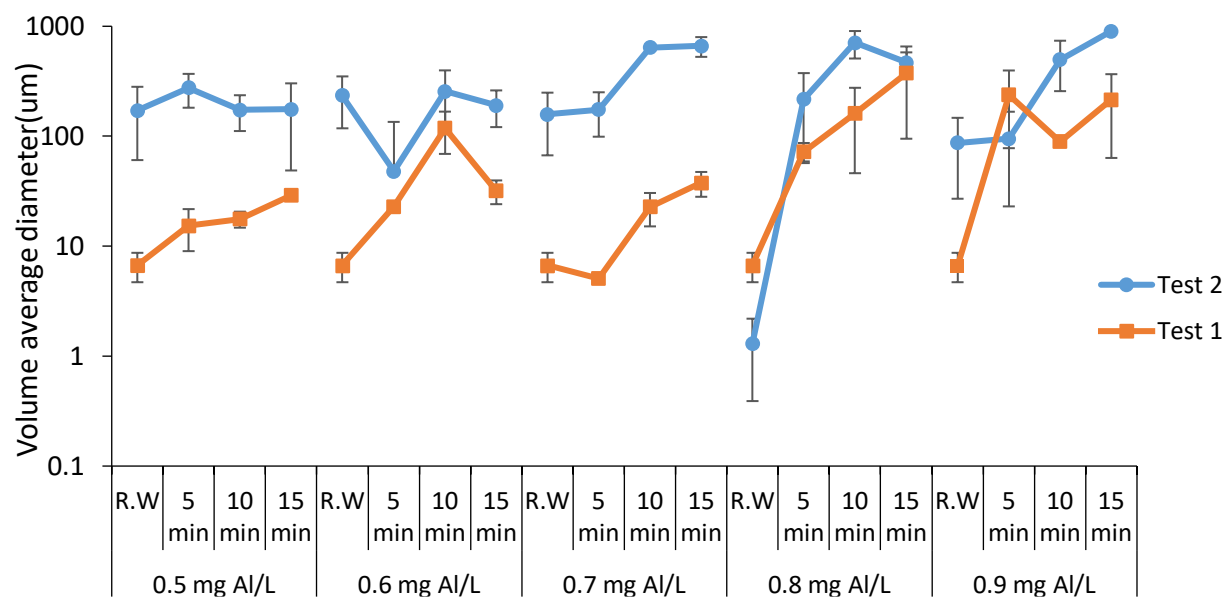


Figure 5-12. Results of floc diameter measurement employing Mastersizer 3000

One of the important factors that can explain these contrast results, is the presence of a high-shear mixer inside the sample container, with the lowest mixing intensity of 500 RPM (shown in

the Figure 5- 13). Since the flocs are pretty shear sensitive, this could make the results unreliable. So, due to the contradicting results, this method was not considered for the rest of this project.

Figure 5- 13. Mastersizer 3000



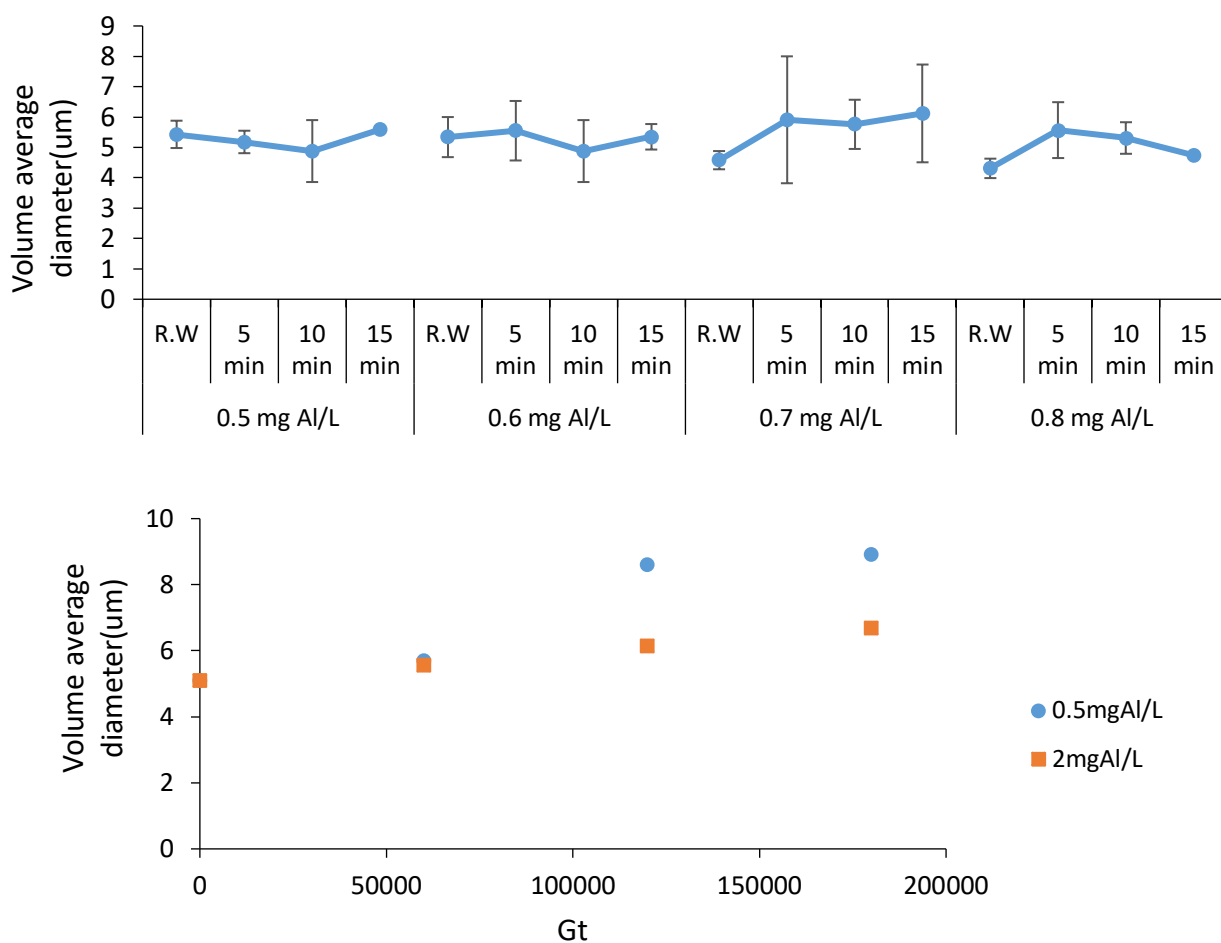
5.2.2 Direct Photometric Analyzer (Brightwell)

The second method employed for floc measurement involved the use of Brightwell Technologies INC's DPA 4100 Flow Microscope. The testing procedure is detailed in the provided Table 5- 4, and the results of three tests are depicted in Figure 5- 14 and Figure 5- 15. This method was previously used in our group to characterize floc size (Ball et al., 2011)

For the dosage range of 0.5-0.8 mg Al/L, at different mixing times, the average floc diameter was consistently less than 10 μm . In a subsequent series of tests, both the G value and dosage were doubled ($G=100 \text{ s}^{-1}$ and dosage=2 mg Al/L). Surprisingly, the average floc diameter remained under 10 μm . However, it is important to note that the Brightwell equipment in CREDEAU, which was installed in 2009, has only one available cell for measurements. Therefore, there was no opportunity to attempt measurements using a different cell. It was assumed that the device's functionality may have been compromised due to its age, especially that we formerly were able to measure flocs of 10-100 μm under similar test conditions. Unfortunately, this method was also unaccepted for the floc measurement.

Table 5- 4. Bright well test protocol

Test Protocol
PAX-XL 1900: 0.5 – 0.8 mg Al/L
Mixing intensity: 50 & 100 rpm
Mixing time: 5 – 15 min
Raw Water DOC: 3.5 mg C/L

Figure 5- 14. Results of floc diameter measurement employing Brightwell ($G=50\text{ s}^{-1}$)Figure 5- 15. Results of floc diameter measurement employing Brightwell ($G=100\text{ s}^{-1}$)

5.2.3 Microscopy

Given that the Laser Diffraction particle analyzer and Direct Photometric Analyzer were unable to measure the flocs, the Olympus BX51 microscope was employed as an alternative method. The testing procedure is outlined in Table 5-5. Samples were first stained with methylene blue to enhance visibility under the microscope. The microscope's integrated camera was used to capture images at 100X, then the images were analyzed. The tests were conducted four times, and two series of results are illustrated in Figure 5-16. The average floc diameter for cases with 0.5 mg Al/L and 2 mg Al/L gradually increased from 20 μm in the raw water to 60 μm at a Gt of 75000. The first series of results has been fitted with an logarithmic trendline, resulting in an R^2 value of 0.92. The equation associated with this trendline, illustrating the relationship between Gt and floc diameter, is displayed on the graph.

Table 5-5. Microscope test protocol

Test Protocol
PAX-XL 1900: 0.5mg Al/L, 2mg Al/L
Mixing intensity: 50 rpm
Mixing time: 5 to 25 min
Stain the sample: Methylene Blue
Raw Water DOC: 3.5 mg C/L

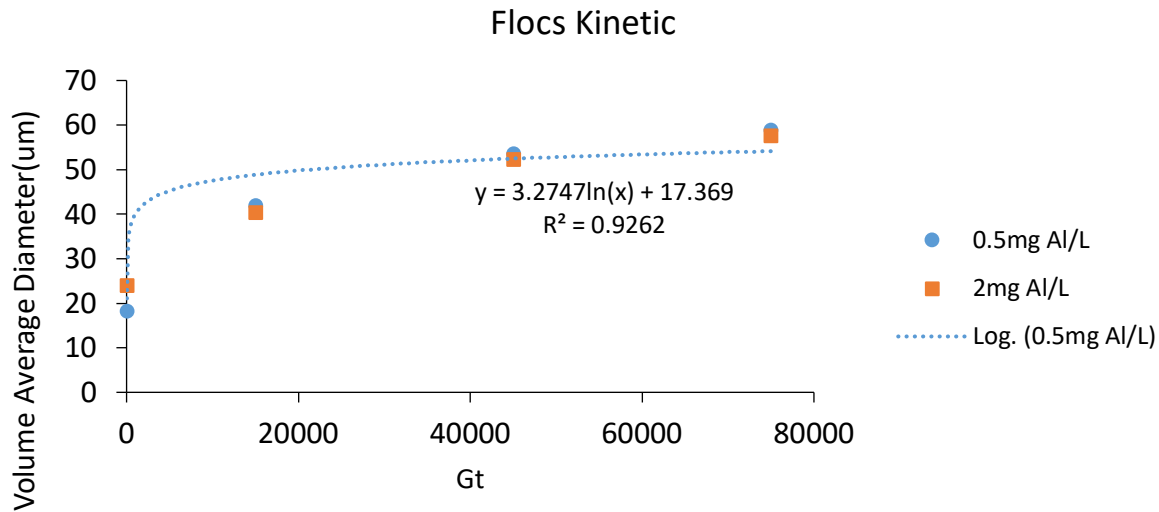


Figure 5-16. Results of floc diameter measurement employing microscopy

5.3 Results

One of the primary objectives of this study is to predict the size of flocs at the outlet of the flocculator, and the point of entry into the filters. Achieving this goal involves synthesizing data from our experimental investigation with Gt values obtained through simulations. The predicted relation between Gt and flocs diameter shown in the Figure 5-16 is employed to predict the flocs distribution through the whole channel. As it is depicted in Figure 5- 17 and Figure 5-18, the floc diameters in both channels vary within the range of 30 to 60 µm. However, in the channel with 16 baffles, there is a gradual increase in floc size, and larger flocs in the range of 50 to 60 µm tend to be more compact towards the end of the flocculator. In contrast, the flocculator with 8 baffles has larger flocs in the range of 45 to 50 µm dispersed throughout the channel, specially in the initial part of the channel in areas of recirculation which has high Gt.

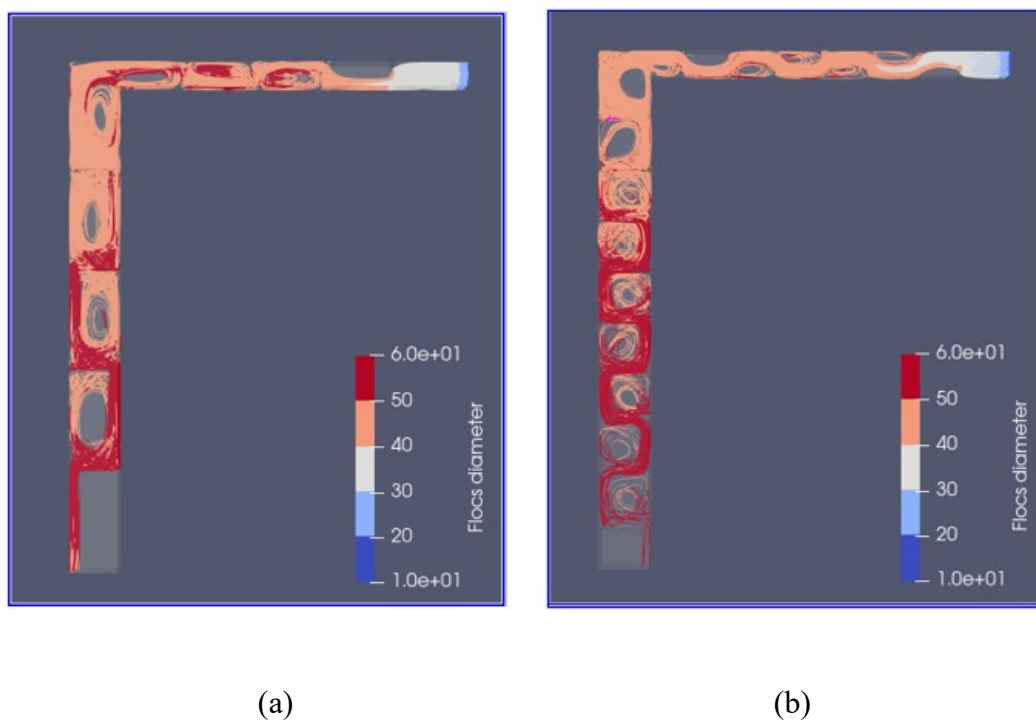


Figure 5- 17. Floc diameter (μm) distribution in the flocculator (a) with 8 baffles (b) with 16 baffles

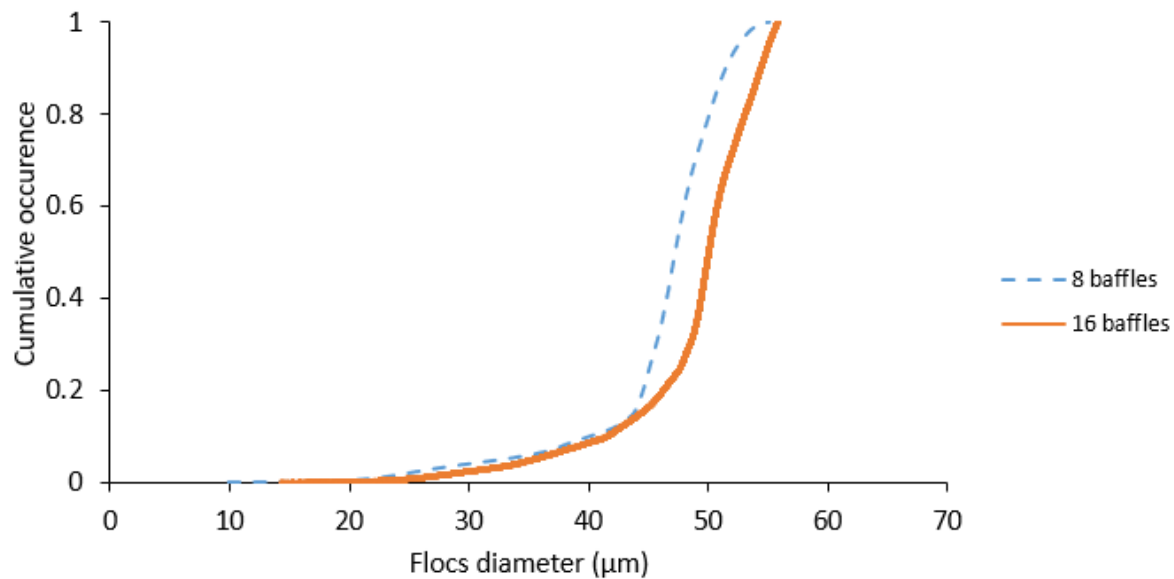


Figure 5-18. Cumulative frequency distribution of flocs diameter in the flocculator with baffle

Additionally, Ball, Carriere, and Barbeau (2011) conducted a similar experiment using low turbidity water from the St. Lawrence River, employing a different coagulant (Alum), and derived a graph illustrating the correlation between floc diameter and Gt. The Gt from the simulation was used to predict the size of the floc using the results of both experimental results. Table 5-6 presents the potential flocs diameter based on the results of both experimental studies for comparison.

The results of this study indicate that, for a channel with 8 baffles and a predicted average Gt of 26000 at the exit of the flocculator, the anticipated floc sizes are estimated to fall within the range of 40 – 45 μm . Conversely, for a channel with 16 baffles and an average Gt of 53000 at the flocculator exit, the projected flocs are expected to range between 50 – 60 μm . This comparison demonstrates that the channel with 16 baffles with higher Gt will lead to the formation of larger flocs.

Additionally, considering the findings of Ball et al. (2011), for a channel with 8 baffles, flocs size is estimated to fall within the range of 20 – 25 μm . Moreover, for the channel with 16 baffles the predicted flocs are expected to range between 40 – 45 μm .

Table 5-6. The predicted floc size at the end of the flocculator

	Predicted Gt_{Ave} (End of the flocculator)	Predicted average flocs diameter	
		(Present study)	(Ball, and Barbeau, 2011)
Channel without baffle	Less than 10000	15 μm	10 μm
Channel with 8 baffles	26000	40 – 45 μm	20 – 25 μm
Channel with 16 baffles	53000	50 – 60 μm	40 – 45 μm

In summary, the findings illustrate that the channel with 16 baffles provides better flow control in terms of Gt and leads to larger anticipated floc sizes compared to the channel with 8 baffles. However, it's crucial to consider that the construction costs for the 16-baffle configuration are much higher. Moreover, it would be important to validate if the predicted differences in floc size have a significant impact on the performance of the filters, an objective that can only be conducted at pilot-scale. Therefore, the choice between the two configurations should weigh the benefits of improved performance against the higher investment required for implementation.

CHAPTER 6 Conclusion and recommendations

6.1 Conclusion

In conclusion, this study aimed to introduce a hydraulic flocculator to enhance the efficiency of the Des-Baillets water treatment plant during periods of peak turbidity. The research employed OpenFOAM for the numerical analysis of the hydraulic flocculator for channels with 8 and 16 baffles, and experimental work to achieve floc growth kinetics. The CFD simulations underwent validation through mesh independence tests and residual analysis, ensuring the accuracy of the results. The main conclusion of this study is presented in the following sections:

1. It is demonstrated that the addition of baffles in the channel after the control valve can create the necessary head loss for hydraulic flocculation. However, it is noteworthy to highlight that the calculated head loss, as determined by OpenFOAM, reveals a slightly higher head loss of 1.2 meter, exceeding the design target head loss utilized in the baffles' design, which stands at 0.75 meters.
2. The velocity analysis indicates differences in flow pattern and recirculation length between channels with 8 and 16 baffles. The 16-baffle configuration demonstrates a more consistent and controlled flow regime, contrasting the 8-baffle channel with its abrupt velocity changes. This distinction may influence shear rates, potentially impacting overall flocculation efficiency.
3. In the channel with 8 baffles, the wide range of velocity gradient (G value) spans from 10 s^{-1} to over 1000 s^{-1} . On the other hand, in the channel with 16 baffles, the G value range extends up to 500 s^{-1} , with nearly half falling within the range of 100 s^{-1} to 220 s^{-1} . The presence and number of baffles significantly influence the flow characteristics, indicating that the 16-baffle configuration leads to a more controlled flow environment with a narrower range of velocity gradient values.

4. Qualitative assessment of Camp number (Gt) illustrates the noticeable increase in Gt after adding baffles. The channel with 16 baffles is experiencing higher Gt values compared to the channel with 8 baffles. In the end of the flocculator where the flow enters the filters, the channel featuring 8 baffles displays an average Gt of 26,000. In contrast, the configuration with 16 baffles presents a higher mean value of 53,000, aligning with the lower range of typically used Gt . Moreover, the reduced variability in Gt of the channel with 16 baffles indicates increased efficiency in the flocculation process.
5. The experimental part of the study, however, encountered challenges in measuring floc sizes using the Mastersizer 3000 and Brightwell's DPA 4100 due to high shear mixing and potential equipment aging issues, respectively. The microscopy method provided more reliable results, showing an increase in floc diameter with an increase in the Gt value.
6. This study aims to predict floc size distribution at the flocculator by combining experimental data with Gt values from simulations. Predicted floc diameters in both channels range from 30 to 60 μm , while the 16-baffle channel exhibits a gradual increase in larger flocs (50–60 μm) toward the end of flocculator. The 8-baffle channel has dispersed larger flocs (45–50 μm), especially in recirculation areas with high Gt .

However, it's important to note that the choice between the two configurations should not solely be based on performance improvement aspects and should also take construction costs into account and the benefits to the filtration process performance. The 16-baffle design, while offering enhanced flow control, comes with higher construction costs. Moreover, validating the impact on filter performance requires pilot-scale testing, emphasizing the need for a balanced decision between improved performance and increased investment.

6.2 Recommendations

Based on the conclusions established in the present study, considering both the results of the numerical model and experimental study the following is recommended:

1. Explore and analyze the impact of different baffle configurations in hydraulic flocculators. Investigate how varying the arrangement, size, shape or type of baffles influences flow patterns, head loss, and ultimately, flocculation efficiency.

2. Extend the investigation to a larger scale, possibly through pilot-scale testing. Assess the scalability of the hydraulic flocculator design and evaluate its performance under conditions that mimic real-world water treatment plant operations.
3. Explore advanced measurement techniques for floc size analysis. Investigate the use of cutting-edge technologies or methodologies that can overcome the challenges encountered in the experimental phase of the study.

REFERENCES

- Amirtharajah, A., & O'melia, C. R. (1990). Coagulation processes: destabilization, mixing, and flocculation. *MCGRAW-HILL, INC.,(USA). 1194*, 1990.
- Andoh, R. (2006). CFD Saves \$50,000 in design of stormwater separator. *Hydro International, Portland, Maine, USA. Fluent News Summer*.
- AWWA. (1980). The status of direct filtration. *Journal (American Water Works Association)*, 405-411.
- Ball, T., Carriere, A., & Barbeau, B. (2011). Comparison of two online flocculation monitoring techniques for predicting turbidity removal by granular media filtration. *Environmental technology*, 32(10), 1095-1105.
- Bernhardt, H., & Schell, H. (1993). Effects of energy input during orthokinetic aggregation on the filterability of generated flocs. *Water Science and Technology*, 27(10), 35-65.
- Bilde, K. G., Hærvig, J., & Sørensen, K. (2023). On the design of compact hydraulic pipe flocculators using CFD-PBE. *Chemical Engineering Research and Design*, 194, 151-162.
- Bouchard, L. (2017). *DÉVELOPPEMENT D'OUTILS POUR L'ÉVALUATION DE LA PERFORMANCE DES PROCÉDÉS DE FILTRATION EN LIGNE ET D'OZONATION DE L'USINE CHARLES-J.-DES BAILLETS*. (DIPLÔME DE MAÎTRISE EN INGÉNIERIE). UNIVERSITÉ DE MONTRÉAL,
- Bouyer, D., Line, A., Cockx, A., & Do-Quang, Z. (2001). Experimental analysis of floc size distribution and hydrodynamics in a jar-test. *Chemical Engineering Research and Design*, 79(8), 1017-1024.
- Brakalov, L. (1987). A connection between the orthokinetic coagulation capture efficiency of aggregates and their maximum size. *Chemical Engineering Science*, 42(10), 2373-2383.
- Bridgeman, J., Jefferson, B., & Parsons, S. A. (2009). Computational fluid dynamics modelling of flocculation in water treatment: A review. *Engineering Applications of Computational Fluid Mechanics*, 3(2), 220-241.
- Bridgeman, J., Jefferson, B., & Parsons, S. A. (2010). The development and application of CFD models for water treatment flocculators. *Advances in Engineering Software*, 41(1), 99-109.
- Camp, T. R. (1943). Velocity gradients and internal work in fluid motion. *J. Boston Soc. Civ. Eng.*, 30, 219-230.
- Crittenden, J. C., Trussell, R. R., Hand, D. W., Howe, K. J., & Tchobanoglous, G. (2012). *MWH's water treatment: principles and design*: John Wiley & Sons.
- Culp, R. L. (1977). Direct filtration. *Journal-American Water Works Association*, 69(7), 375-378.

- Dalsasso, R. L., & Sens, M. L. (2006). Filtração direta com pré-floculação e coagulação com sulfato de alumínio e hidróxido de alumínio: Estudo com água de manancial eutrofizado. *Engenharia Sanitária e Ambiental*, 11, 241-249.
- de Oliveira, D. S., & Donadel, C. B. (2019). Global velocity gradient evaluation: An innovative approach using CFD modeling applied to water and wastewater treatment plants. *Journal of Water Process Engineering*, 28, 21-27.
- Ducoste, J. J., & Clark, M. M. (1998). The influence of tank size and impeller geometry on turbulent flocculation: I. Experimental. *Environmental Engineering Science*, 15(3), 215-224.
- Ducoste, J. J., Clark, M. M., & Weetman, R. J. (1997). Turbulence in flocculators: effects of tank size and impeller type. *AIChE journal*, 43(2), 328-338.
- Edzwald, J. K., Becker, W. C., & Tambini, S. J. (1987). Organics, polymers, and performance in direct filtration. *Journal of Environmental Engineering*, 113(1), 167-185.
- Egarr, D., Horton, L., Rice, H., & Hunter, T. (2016). 10TH EUROPEAN WASTE WATER CONFERENCE DEVELOPMENT OF FLOCCULATION MODELS FOR IMPROVING WATER TREATMENT.
- Fitzpatrick, C., Fradin, E., & Gregory, J. (2004). Temperature effects on flocculation, using different coagulants. *Water Science and Technology*, 50(12), 171-175.
- Ghawi, A. H. (2018). Optimal design parameters for hydraulic vertical flocculation in the package surface water treatment plant. *Przegląd Naukowy Inżynieria i Kształtowanie Środowiska*, 28.
- Haarhoff, J. (1998). Design of around-the-end hydraulic flocculators. *Journal of Water Supply: Research and Technology—AQUA*, 47(3), 142-152.
- Haarhoff, J., & van der Walt, J. J. (2001). Towards optimal design parameters for around-the-end hydraulic flocculators. *Journal of Water Supply: Research and Technology—AQUA*, 50(3), 149-160.
- Han, M., & Lawler, D. F. (1992). The (relative) insignificance of G in flocculation. *Journal-American Water Works Association*, 84(10), 79-91.
- ImagJ. (2005). Retrieved from <https://imagej.net/imagej-wiki-static/Downloads.html>
- Jarvis, P., Jefferson, B., Gregory, J., & Parsons, S. A. (2005). A review of floc strength and breakage. *Water research*, 39(14), 3121-3137.
- Joodi, A. S. (2013). Effect of baffles geometry of the flocculation basin on the turbulence behavior using Comsol multiphysics technique. *Journal of Environmental Studies*, 10(1), 71-77.
- Kawamura. (2000). *Integrated design and operation of water treatment facilities* (Second ed.). New York, USA: John Wiley and Sons, Inc.
- Kurniawan, S. B., Abdullah, S. R. S., Imron, M. F., Said, N. S. M., Ismail, N. I., Hasan, H. A., . . . Purwanti, I. F. (2020). Challenges and opportunities of biocoagulant/bioflocculant application for drinking water and wastewater treatment and its potential for sludge

- recovery. *International journal of environmental research and public health*, 17(24), 9312.
- McEwen, J. B. (1998). *Treatment process selection for particle removal*: American Water Works Association.
- Melo, L. D. V., Barroso, G. R., Figueiredo, R. S., Costa, E. P., & Oliveira, S. C. (2021). Applicability of statistical analysis for performance and reliability evaluation of large-scale water treatment plants with direct filtration systems. *Environmental Science and Pollution Research*, 28, 22427-22438.
- Melo, P., Freire, E., Ansoni, J., Oliveira, L., & Franco, C. (2022). Velocity gradient optimization in a perforated tray-type flocculator using OpenFOAM: CFD as a tool in water treatment. *Journal of Applied Fluid Mechanics*, 15(2), 387-397.
- Moin, P. (2010). *Fundamentals of engineering numerical analysis*: Cambridge University Press.
- Moukalled, F., Mangani, L., Darwish, M., Moukalled, F., Mangani, L., & Darwish, M. (2016). *The finite volume method*: Springer.
- National.Geographic. (2023). Earth's fresh water. Retrieved from <https://education.nationalgeographic.org/resource/earths-fresh-water/>
- OpenFOAM-Guide, U. (2020). OpenFOAM. *no. June*.
- OpenFOAM. (2022). Retrieved from <https://openfoam.org/download/>
- ParaView. (2023). Retrieved from <https://www.paraview.org/download/>
- Post, G., Atherholt, T., & Cohn, P. (2011). Water quality and treatment: a handbook on drinking water. *Health and aesthetic aspects of drinking water*, 6th edn. McGraw-Hill, New York, 2.1-2.100.
- S.Carlston, J. (2015). IMPACT OF GEOMETRIC DESIGN OF HYDRAULIC CONTACT TANKS ON RESIDENCE TIME DISTRIBUTIONS.
- Saha, S., Biswas, P., Nath, S., & Singh, L. (2021). Numerical simulations of Newtonian fluid flow through a suddenly contracted rectangular channel with two different types of baffle plates. *Soft Computing*, 25(15), 9873-9885.
- SALOME-platform. (2019). SALOME. Retrieved from <https://www.salome-platform.org/wp-content/uploads/2022/01/SALOME9-brochure.pdf>
- SALOME, V. (2021). Retrieved from <https://www.salome-platform.org/?p=2176>
- Schwer, L. E. (2008). Is your mesh refined enough? Estimating discretization error using GCI. *7th LS-DYNA Anwenderforum*, 1(1), 45-54.
- Shaw, C. T. (1992). Using computational fluid dynamics. (*No Title*).
- Thomas, D., Judd, S., & Fawcett, N. (1999). Flocculation modelling: a review. *Water research*, 33(7), 1579-1592.
- Treweek, G. P. (1979). Optimization of flocculation time prior to direct filtration. *Journal-American Water Works Association*, 71(2), 96-101.

- Van der Walt, J. J. (2002). *The modelling of water treatment process tanks*. University of Johannesburg,
- Vigneswaran, S., Notthakun, S., & Thanh, N. (1984). Flocculation time optimization in direct water filtration. *Effluent & water treatment journal*, 24(7), 270-274.
- Von Smoluchowski, M. (1917). Versuch einer mathematischen Theorie der Koagulationskinetik. *Phys. Chem*, 92, 156.
- WHO. (2019). World Health Organisation, UNICEF. Retrieved from <https://www.who.int/news/item/18-06-2019-1-in-3-people-globally-do-not-have-access-to-safe-drinking-water-unicef-who>
- Yeung, H. (2001). Modelling of service reservoirs. *Journal of Hydroinformatics*, 3(3), 165-172.
- Zarchi, I., Friedler, E., & Rebhun, M. (2013). Polyaluminium chloride as an alternative to alum for the direct filtration of drinking water. *Environmental Technology*, 34(9), 1199-1209. doi:10.1080/09593330.2012.743594